Publishing Office: *Department of Industrial Engineering, Engineering Faculty, King Abdulaziz University, P.O. Box: 80204 Jeddah 21589 Saudi Arabia*; Tel: +966 533 107628; Fax: +966 2 2486695.

Frequency: Journal of International Environmental Application and Science (ISSN 2636-7661) is published 4 times per year.

Aims and Scope: Journal of International Environmental Application and Science is dedicated to detailed and comprehensive investigations, analyses and appropriate reviews of the interdisciplinary aspects of renewable sources, municipal and industrial solid wastes, waste disposal, environmental pollution, environmental science and education, biomass, agricultural residues, energy sources, hazardous emissions, incineration, environmental protection topics included experimental, analytical, industrial studies, hydrological recycling, water pollution, water treatment, air pollution, gas removal and disposal, environmental pollution modelling, noise pollution and control. Suitable topics are also included regarding the efficient environmental management and use of air, water and land resources.

Publication information: Please address all your requests regarding orders and subscription queries to: *Dr. S. Dursun*, Environmental Engineering Department, Engineering Faculty, Konya Technical University, Konya, TURKEY. Tel: +90 3332 2051559, Fax: +90 332 2410635, Mobil: + 90 536 5954591.
E-mail: jieas@jieas.com

Guide for Authors

Submission of Papers: Manuscripts for publication may be sent to the Editor-in-Chief, a member of the Editorial Board. Submission address is: Editor-in-Chief, Dr. S. Dursun, Environmental Engineering Department, Engineering & Natural Science Faculty, Konya Technical University, Konya, TURKEY. Manuscripts can also be sent to any member of the Editorial Board (see inside front cover for addresses). Although this journal is international in scope, all articles must be in the English language. Potential contributors whose first language is not English are urged to have their manuscript competently edited prior to submission. Papers should be written in the third person in an objective, formal and impersonal style.

Manuscript Preparation:

General: Manuscripts must be typewritten, double-spaced with wide margins on one side of white paper. Good quality printouts with a font size of 12 pt are required. The corresponding author should be identified (include E-mail address, Telephone and Fax number). Full postal addresses must be given for all co-authors. Two hard copies of the manuscript should be submitted by regular mail.

Abstracts: Each manuscript must be including a brief abstract and a short list of keywords.

Text: Follow this order when typing manuscripts: Title, Authors, Affiliations, Abstract, Keywords, Introduction, Main text, Conclusion, Acknowledgements, Appendix, References, Vitae and Figure Captions followed by the Figures and Tables. Pages should be numbered consecutively. The corresponding author should be identified with an asterisk and footnote.

Symbols and Units: All Greek letters and unusual symbols should be identified by name in the margin, the first time they are used. SI units should be used wherever possible, as recommended in ISO 1000 and BS 5555.

References: All publications cited in the text should be presented in a list of references following the text of the manuscript. In the text refer to the author's name (without initials) and year of publication (*e.g.* "since Dursun (1993) has shown that..." or "This is in agreement with results obtained later (Boddy, 1984)". For three or more authors use the first author followed by "*et al.*", in the text. The list of references should be arranged alphabetically by authors' names. The manuscript should be carefully checked to ensure that the spelling of authors' names and dates are exactly the same in the text as in the reference list.

References should be given in the following form:

Boddy L, (1984) The micro-environment of basidiomycete mycelia in temperate deciduous woodlands. In: *The Ecology and Physiology of the Fungal Mycelium* (Ed. by D.H. Jennings & A.D.M. Rayner), pp. 261-289. British Mycological Society Symposium 8, Cambridge University Press, Cambridge.

Dursun S, Ineson P, Frankland JC, Boddy L, (1993) Sulphite and pH effects on CO_2 evolution from decomposing angiospermous and coniferous tree leaf litters. *Soil Biology & Biochemistry* **25**, 1513-1525.

Ergas SJ, Schroeder E, Chang D, Scow K, (1994) Spatial distributions of microbial populations in biofilters. In: Proceedings of the *78th Annual Meeting and Exhibition of the Air and Waste Management Association*, pp. 19-24, Cincinnati, OH.

Hickey M, King C, (1988) *100 Families of Flowering Plants*. Cambridge University Press, Cambridge.

Littlejohn D, Wang Y, Chang S-G, (1993) Oxidation of aqueous sulphite ion by nitrogen dioxide. *Environmental Science & Technology* **27**, 2162-2167.

Illustrations: All illustrations should be provided in camera-ready form, suitable for reproduction (which may include reduction) without retouching. Photographs, charts and diagrams are all to be referred to as "Figure" and should be numbered consecutively in the order to which they are referred. They should be accompanying the manuscript, should be included within the text.

Tables: Tables should be numbered consecutively and given a suitable caption and each table should be included within the text. Footnotes to tables should be typed below the table and should be referred to by superscript lowercase letters.

Electronic Submission: Authors may submit electronic copy of their manuscript by e-mail or online submission on WEB site of the JIEAS. The final version of the manuscript should be submitted on floppy disk or CD. The electronic copy should match the hardcopy exactly. MS Word is recommended for software for article submission.

Proofs: Proofs will send to the author and should be returned 48 hours of receipt. Corrections should be restricted to typesetting errors; any others may be charged to the author. Any queries should be answered in full.

Subscription: Subscription for the issue contains author's article published in "*Journal of International Environmental Application and Science*" is €100.00 which will be sending to the corresponding author. Journal of International Environmental Application and Science (ISSN 1307-0428) is published since 2006. Subscription rates for a year are Institutions: € 300.00 (four issues per a year) Individuals: € 150.00 (four issues per a year)

Copyright: Papers are considered for publication on the understanding that they have not been submitted to any other publisher. Except for review papers, the work described must be original and, generally speaking, not previously published. Authors who wish to reproduce illustrations that have been published elsewhere must obtain the permission of the copyright holder.

Correspondence: Papers should be sent to: *Dr. S. Dursun*, *Environmental Engineering Department, Engineering Faculty, Selcuk University, Konya, Turkey*. It may also be sent by e-mail to jieas@jieas.com in Microsoft Office Word 2007 format.

Website**:** *http://www.jieas.com;* ***E-Mail****: jieas@jieas.com, info@jieas.com*

"Journal of International Environmental Application and Science" is indexed in:
"**Global Impact Factor**, **EBSCO, CAS Source Index (A Division of the American Chemical Society), Index Copernicus, ProQuest, CABI, Ulrich's™ Serials Analysis System, SCIRUS, ArgosBiotech, NAAEE, The University of Queensland's Institutional, The NAL Catalog (AGRICOLA), WORLDCAT Catalog, LexisNexis, The National Library of Finland, National Library of Australia, DergiPark Turkey"** *Journal Indexing List.*

C O N T E N T S

J. Int. Environ. Appl. & Sci., Vol. 19 No. 3 pp: 121-159 September 2024

J. Int. Environmental Application & Science, Vol. **19**(3): 121-150 (2024)
Research Paper

Assessing Aquifer Vulnerability to Cemetery Contamination Using Geophysical and Geotechnical Techniques

Ilaboya, Idowu Rudolph[1, *]; Omosefe, Eghosa Blessing[2] Ambrose-Agabi, Enoredia Esther[3],

[1, 2,3,] *Department of Civil Engineering, Faculty of Engineering, University of Benin, Benin City, Nigeria*

Received June 19;2024; Accepted July 10, 2024

Abstract: In this study, an integrated geotechnical and geophysical investigation of the second cemetery in Benin City was conducted. The primary objective was to determine the hydraulic properties of the underlying formation to assess the potential transmission of necroleachate. Eight vertical electrical soundings (1-D VES) and two dipole-dipole profiling lines along two transverse sections were carried out. For the dipole-dipole profiling, ABEM Terrameter SAS 300C was employed, while the VES investigation utilized the Schlumberger array. The resistivity data collected during the field study were interpreted using DIPROWIN software version 4.01 while the geotechnical properties such as moisture content and bulk density were conducted in accordance with BS1377: part 2: 1990 and BS EN 1997-2:2007. According to the dipole-dipole results, the leachate plume was identified in the subsurface soil at a depth range of 5 to 20 meters. This presence is likely attributed to the high level of porosity, facilitating the infiltration and percolation of necroleachate into the underlying soil. The VES results revealed four geoelectric layers: topsoil, lateritic soil, a weathered layer (composed of clay), and medium to coarse sand. The overburden exhibited a thickness range of 0.7762m to 0.8074m, resistivity ranging from 57.318Ωm to 2831.4Ωm, and depth ranging from 0.7762m to 1.5836m. The third geoelectric layer, identified as clay, had an average thickness of 11.48 meters at a depth of 13.06 meters, with a resistivity of 203.52Ωm. Apart from acting as a seal against the vertical penetration of leachate into the underlying aquifer, the clay also serves as a filter for leachate resulting from the decomposition of dead bodies.

Keywords: *Vertical Electrical Sounding, Dipole-Dipole profiling, Aquifer vulnerability, necroleachate contamination, Cemetery activities*

Introduction

Safe water is defined as water that meets the national standards for drinking water quality (NSDWQ) (Adeyeye & Abulude, 2004). Access to safe drinking water is crucial for poverty reduction and serves as a strategic measure to prevent the spread of waterborne and sanitation-related diseases (Kudesia & Kudesia, 2008; Eugeniusz et al., 2017). Groundwater, constituting about 30% of the world's readily available fresh water supply, is a major water source (Asadi et al., 2007). It meets the needs of approximately 30% of the global population (Asadi et al., 2007). Although water exists in three different states, the water that is available to man usually comes from two main sources viz; surface water and groundwater. Groundwater, simply put, is water located beneath the ground surface in soil pore spaces and rock formations' fractures. Its primary source is the infiltration of precipitation into the ground following rainfall (Eugeniusz *et a*l., 2017), making aquifers reliant on rainfall for recharge. The reliance on groundwater arises from challenges associated with surface water, such as scarcity and pollution (Debels *et al.*, 2005; Priyan, 2021; Sahoo & Khaoash, 2020). Despite instances of mediated contamination as groundwater traverses rock formations, anthropogenic influences have heightened groundwater's susceptibility to contamination (Sahoo & Khaoash, 2020).

For many communities worldwide, groundwater serves as a crucial natural resource and the primary source of drinking water (Gleeson et al., 2016). However, various anthropogenic activities, including waste disposal practices associated with cemetery activities, pose a potential risk of contaminating groundwater resources (Üçisik & Rushbrook, WHO, 1998; Żychowski, 2012; Bastianon *et al.*, 2000). In numerous urban areas, particularly in developing countries, cemeteries are often situated in locations where groundwater supplies are vulnerable to contamination, often adjacent to residential areas (Lautz et al., 2020; Trick et al., 2005). In Nigeria, cemetery operations frequently

*Corresponding: E-Mail: rudolph.ilaboya@uniben.edu, Tel: +2348038027260

proceed without proper management procedures, leading to the release of leachate from decomposed organic matter and other waste items into the environment. Groundwater contamination resulting from cemetery activities can have severe consequences for both the ecosystem and public health (Trick et al., 2005). This raises significant concerns regarding the susceptibility of aquifers to contamination due to cemetery activities, particularly in metropolitan areas where the demand for water is substantial (Abu-Bakr & El-A., 2020; Bon *et al.*, 2020; Ekanem, 2020; Ekanem et al., 2019; Aleke *et al*., 2018).

The most potentially sensitive receiver of contaminants from graves is identified as groundwater. The decomposition of deceased individuals and funeral items in cemeteries introduces biological contaminants, such as bacteria and viruses, into the environment (Dian, 2004). Studies indicate that the ecology may suffer due to poorly placed cemeteries and a lack of measures to prevent the transfer of contaminants into the underlying aquifer (Kabiru *et al*., 2019). Aquifer protection hinges on the permeability of the underlying medium, influencing the transmission of contaminants into subordinate aquifer units (Egbai et al., 2019; Oseji and Egbai, 2019a). The rate and amount of leachate intrusion are primarily determined by how easily contaminants can travel through the subsurface strata beneath the cemetery and its surroundings. While less permeable clayey materials act as a geological barrier restricting the transport of contaminants, permeable sandy materials facilitate the easy entry of contaminants, as reported by Olla et al., 2015; Ayuk *et al*., 2013; Awoniyi, 2013. To assess the impact of nearby cemeteries on the underlying aquifer system, understanding the subsurface soil profile is crucial (Omosuyi & Oseghale, 2012). It's essential to note that cleaning up and restoring an aquifer to its original, pristine form is often challenging once it has been polluted (Thirumalaivasan 6 Karmegam, 2001). Therefore, conducting an aquifer vulnerability assessment is crucial to locate potential contamination risk points around cemeteries.

The concept of aquifer vulnerability is based on the idea that groundwater may be protected to some extent from human influences by the physical environment, particularly in terms of contaminants penetrating the subsurface. Aquifer vulnerability combines the strata's potential for attenuation with the saturated zone's hydraulic inaccessibility to the entry of contaminants (Foster, 1998; Eluwole & Ademilua, 2014). To prevent contamination of underlying groundwater supplies, attention might be focused on restricting land use in susceptible zones (Omosuyi & Oseghale, 2012; Awoniyi, 2013). In addition, understanding the direction of leachate flow from decomposing corpses can be a solution to groundwater contamination. Once the flow direction is established, government and relevant agencies should prevent residents along this path from locating boreholes. Geophysical approaches, including electrical resistivity imaging, have shown promise in evaluating aquifers' susceptibility to contamination and locating potential hotspots in the aquifer systems' subsurface geology (Oseji & Egbai, 2019b; Oseji *et al.*, 2019a; Thirumalaivasan & Karmegam, 2001; Anomohanran, 2011). Geophysical approaches serve as effective tools for assessing and defining pollution plumes, observing their changes over time, and facilitating the monitoring of aquifer vulnerability to contamination. Many researchers in the field of environmental engineering have utilized geophysical approaches. For instance, Olla *et al.*, (2015) employed the resistivity approach to evaluate Oleh's groundwater potential. Similarly, Oseji and Egbai (2019a) utilized the resistivity method to assess groundwater prospects and the vulnerability of the overburdened aquifer in Oleh, Delta State, Nigeria. In Irawarea, Lagos State, Ayolabi *et al*. (2013) employed the resistivity method to investigate the aquifer unit and groundwater quality. Others, such as Oseji *et al.* (2018), used the resistivity approach to examine groundwater quality and the impact of several open dumpsites on aquifer preservation in Sapele, Delta State, Nigeria. In Agbor-NTA and its surroundings, Egbai *et al.* (2019) employed the resistivity method to study the aquifer's capacity to withstand damage. Additionally, in Issele-Uku, Delta State, Nigeria, Oseji and Egbai (2019a) conducted an aquifer characterization using geoelectric survey data.

Groundwater contamination from cemetery activities poses significant environmental and public health concerns globally. Assessing the vulnerability of aquifers to such contamination is crucial for effective groundwater management and protection. Integrated geophysical and geotechnical techniques play a pivotal role in this assessment, offering detailed insights into subsurface conditions and pollutant transport pathways. Geophysical methods, including Vertical Electrical Sounding (VES) and Electrical Resistivity Tomography (ERT), are commonly employed to characterize subsurface geological formations around cemetery sites. These techniques provide data on soil resistivity, which correlates with geological features such as clay content and permeability. By mapping subsurface

structures and identifying potential pollutant pathways, geophysical surveys help in understanding how contaminants from cemetery leachates migrate through the aquifer. Complementing geophysical approaches, geotechnical investigations yield essential data on soil properties like hydraulic conductivity, porosity, and moisture content. These parameters influence the movement and attenuation of contaminants in the subsurface. Integrated analysis of geophysical and geotechnical data enables researchers to assess the vulnerability of aquifers to contamination more comprehensively.

Although, the target of this study is to assess the susceptibility of aquifers to leachate contamination from cemetery activities in Benin City, Edo State, Nigeria using electrical resistivity datasets. It also aims to contribute to the development of appropriate management methods for minimizing hazards associated with such activities and provides valuable insights into the potential effects of cemetery activities on groundwater resources.

Leachate Plume Contamination in Relation with Electrical Resistivity Measurement

Geophysical techniques play a crucial role in studying both surface and subsurface contamination caused by various pollutants. Leachates exhibit notable electrical conductivity due to the dissolved salts they contain (Cristina et al., 2012). Given their high ion concentrations and low resistance in rock formations, the electrical resistivity technique is valuable for mapping and locating leachate contamination levels within cemeteries. The transport of pollutants introduced into the environment across porous channels involves four fundamental processes, namely, adsorption, convection, diffusion, and mechanical dispersion. Numerous scholars in the study of soil/groundwater contamination have highlighted these processes (Abdullahi *et al*., 2011; Jegede *et al*., 2012). Adsorption influences the behavior of contaminants in the soil and is considered a primary transport factor regulating pollutant distribution in soil and water-based environments (Ganiyu *et al.*, 2015). Attenuation can occur through processes such as dilution, absorption, ion exchange, precipitation, oxidation/reduction reactions, and breakdown processes, and the efficacy of these processes depends on geological and climatic factors, as well as the quality of the leachates involved. Subsurface weathering and attenuation processes contribute to reducing the potential effects of leachates (Giang *et al*., 2018; Ayolabi *et al.*, 2013). By applying the electrical resistivity approach to geophysical surveys, one can obtain information about the leachate flow direction and Ohm's law can be used to determine the subsurface resistivity since the apparent resistivity is invariably the sum of all the subsurface flux. The following is the basic tenet of Ohm's law:

$$V = IR \tag{1}$$

Where; V is the voltage (v), I; is the current (amp). In this instance, R is not resistance but resistivity; the main reason being that, in contrast to resistance, which is purely dependent on the dimensions of the material, resistivity can actually be linked to density, an essential property. The definition of resistivity is;

$$R = \frac{\rho L}{A} \tag{2}$$

$$V = \frac{I\rho L}{A} \tag{3}$$

For a hemispherical surface, A= $2\pi r^2$

$$V = \frac{I\rho L}{2\pi r^2} \tag{4}$$

$$dV = \frac{I\rho dL}{2\pi r^2} \tag{5}$$

$$\int_0^v dV = I\rho \int_0^r \frac{1}{2\pi r^2} dr \tag{6}$$

$$V = \frac{I\rho}{2\pi r} \tag{7}$$

The potential generated at point M can be estimated as follows;

$$V_{AM} = \frac{I\rho}{2\pi AM} \quad (8)$$

$$V_{BM} = \frac{-I\rho}{2\pi BM} \quad (9)$$

$$V_M = \frac{I\rho}{2\pi}\left[\frac{1}{AM} - \frac{1}{BM}\right] \quad (10)$$

Similarly, the potential generated at point N can be estimated as follows;

$$V_N = \frac{I\rho}{2\pi}\left[\frac{1}{AN} - \frac{1}{BN}\right] \quad (11)$$

Cumulatively,

$$V_{MN} = V_M - V_N = \frac{I\rho}{2\pi}\left[\frac{1}{AM} - \frac{1}{BM} - \frac{1}{AN} + \frac{1}{BN}\right] \quad (12)$$

Where;
ρ; is the resistivity of the soil
I; is intensity of current applied to the soil by electrodes AB (mA),
dV; is differential potential between electrodes MN (mV),

Materials and Methods

Description of Study Area

The study area is the second cemetery in Benin City, Edo State, Nigeria. Benin City, the capital of Edo State, is one of the largest cities in Nigeria, situated in the southern part of the country. It is positioned between latitude 6°20′17″ N and longitude 5°37′32″ E, with an elevation of 88 meters above sea level. Benin City experiences two main seasons: the wet season (March to October) and the dry season (October to March). The city is predominantly inhabited by the Bini-speaking people of Edo ethnic nationality, with a population of 1.15 million persons according to the last national census in 2006. The projected population of the city, using the National Population Commission's growth rate of 3.5% per annum for urban centers, is estimated to reach 5.5 million by the year 2050. There are three main public cemeteries in the city: 1st Cemetery, 2nd Cemetery, and 3rd Cemetery. For this study, the 2nd Cemetery was selected. Figure 1 depicts a 3D-study area map, illustrating the location of the cemetery.

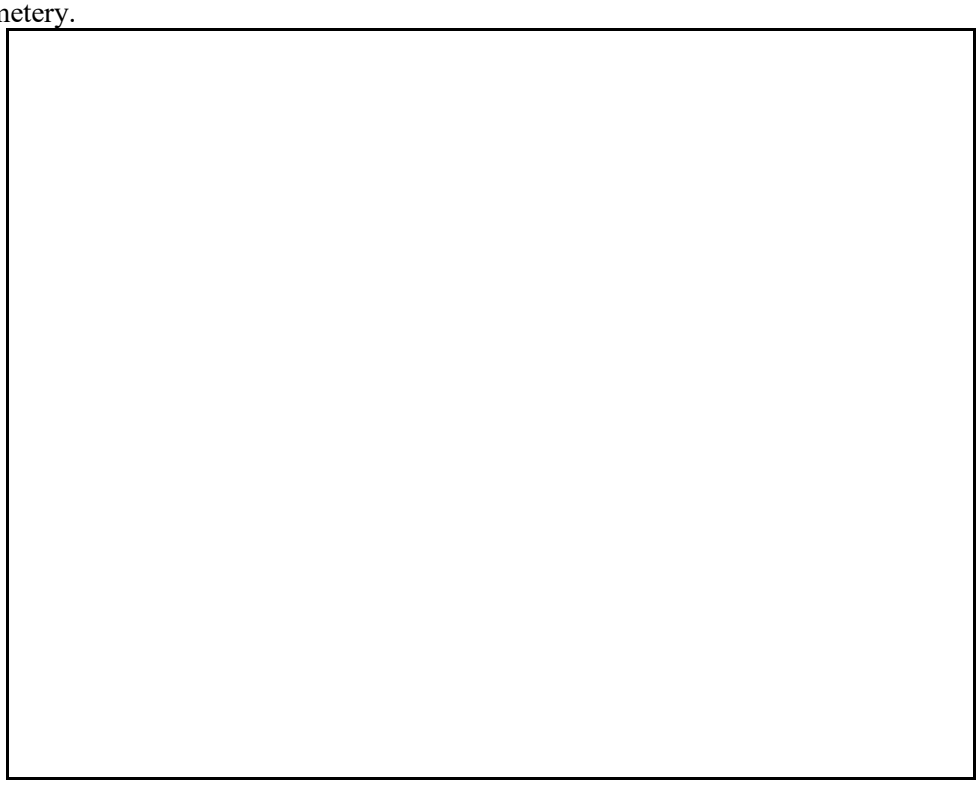

Figure 1. Second cemetery

Geology of the Study Area

The modified geological map of Edo State, presented in Figure 2, shows Benin City and other locations. The Benin region is underlain by sedimentary formations of the South Sedimentary Basin (Ikhile, 2016), extending from the west across the entire Niger Delta area and southward beyond the present coastline. This formation consists of over 90% sandstone with shale intercalations. It is characterized by coarse-grained, gravelly, locally fine-grained, poorly sorted, and sub-angular to well-rounded sediment, bearing lignite streaks and wood fragments (Idehai & Egai, 2014). The general geology is marked by reddish topsoil composed of ferruginized or literalized clay sand.

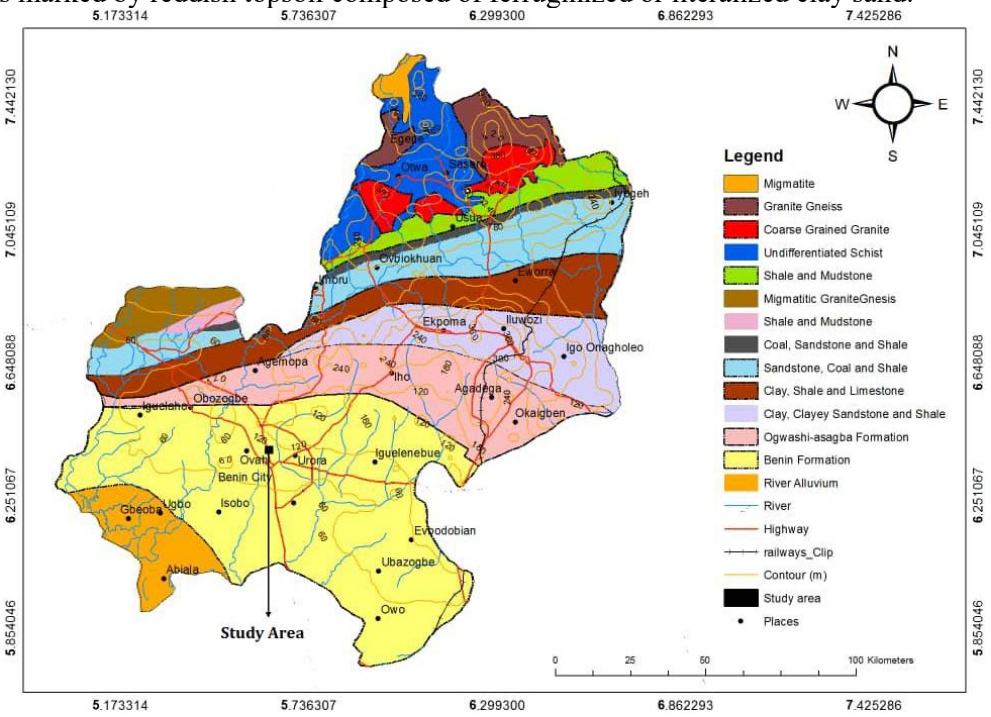

Figure 2 Geology of Benin Formation

Data Collection Procedure

The ABEM Terrameter SAS 300C (Figure 3), GPS for coordinate and elevation measurements, DIPRO application version 4.01 iterative software programs for 2-D resistivity inversion, winRESIST software version 1.0 (a computer-assisted 1-D forward modeling tool), and Surfer Software program for contouring were utilized to conduct the VES and ERT resistivity survey around the second cemetery in Benin City. A combination of geophysical and geotechnical approaches was employed to delineate the geological formation of the subsurface soil around the cemetery, map pollution of the subsoil, and determine the hydraulic properties (mean apparent resistivity, longitudinal conductance, hydraulic conductivity, transverse resistance, conductivity, and transmissivity) of the underlying soil (Orakwe *et al*., 2018; Ugwuanyi *et al*., 2015; Obiora et al., 2016). The electrical resistivity approach involving both 1-D vertical electrical sounding (VES) and 2-D dipole-dipole profiling techniques was adopted for the geophysical investigation while the geotechnical properties such as moisture content and bulk density were determined in line with BS1377: part 2: 1990 and BS EN 1997-2:2007.

Figure 3. ABEM Terrameter SAS 300C

Two transverse lines (TR1-TR2) running in the NE-SW direction, as observed in Figure 4, were established along which 2-D imaging was conducted. Data acquisition for the 2-D imaging was performed using the dipole-dipole array with a dipole length (a) ranging between 0 and 100m and expansion (n) varying from 1-5m according to Orakwe et al. (2018), Lashkaripour and Nakhaei (2005), and Gemail *et al*. (2011). To monitor the current and voltage for each electrode pair, four electrodes were driven into the ground to a depth of 1m using a hammer and a steel pin with a spacing distance of 10m and insulating wires were used to link the electrodes to the resistivity meter (Kearey *et al.*, 2002; Hubbard & Rubin, 2006; Iserhien-Emekeme *et al*., 2004). Direct current was sent into the ground through a pair of current electrodes (A and B), while another pair of potential electrodes (M and N) measured the potential difference created. During this process, the apparent resistance (Ra) of the penetrated geologic materials was read from the crystal display of the resistivity meter (Ogundana *et al*., 2020). The geometrical coefficient (G) of the electrode location for a dipole-dipole array was determined based on the distance between the electrodes using the equation:

$$G = \pi \left[\frac{\left[\left(\frac{AB}{2} \right)^2 - \left(\frac{MN}{2} \right)^2 \right]}{MN} \right] \quad (13)$$

Figure 4. Google earth image of 2nd cemetery showing the two transvers for 2-D imaging

The apparent resistivity (ρa) was calculated by multiplying the apparent resistance (Ra) by the geometric factor G, given by the expression in equation (15) (Kearey *et al*., 2002; Hubbard & Rubin, 2006; Iserhien-Emekeme *et al*., 2004).

$$\rho_a = (GR_a) \quad (14)$$

The DIPRO application version 4.01 was employed to invert the 2-D Dipole-Dipole data into 2-D resistivity profiles. These profiles were crucial for examining subsurface features and identifying probable contamination hotspots. Eight (8) Vertical Electrical Sounding (VES) stations (Figure 5) were conducted using the Schlumberger array, with a maximum current output of 2 amps and a maximum voltage output of 600 volts. Depth sounding curves generated from the VES stations were quantitatively interpreted using winRESIST software version 1.0. This computer-assisted 1-D forward modeling tool utilizes the partial curve matching technique for data interpretation. To investigate the geotechnical properties of the soil within the cemetery location, five boreholes were drilled. Fifteen profile soil samples (PSS1 – PSS15) were collected at depths of 0m, 1m, and 3m, respectively. These samples, stored in black polyethylene bags, were analyzed for specific gravity, moisture content, bulk density, particle size distribution, porosity, and permeability using standard methods and equations presented as follows;

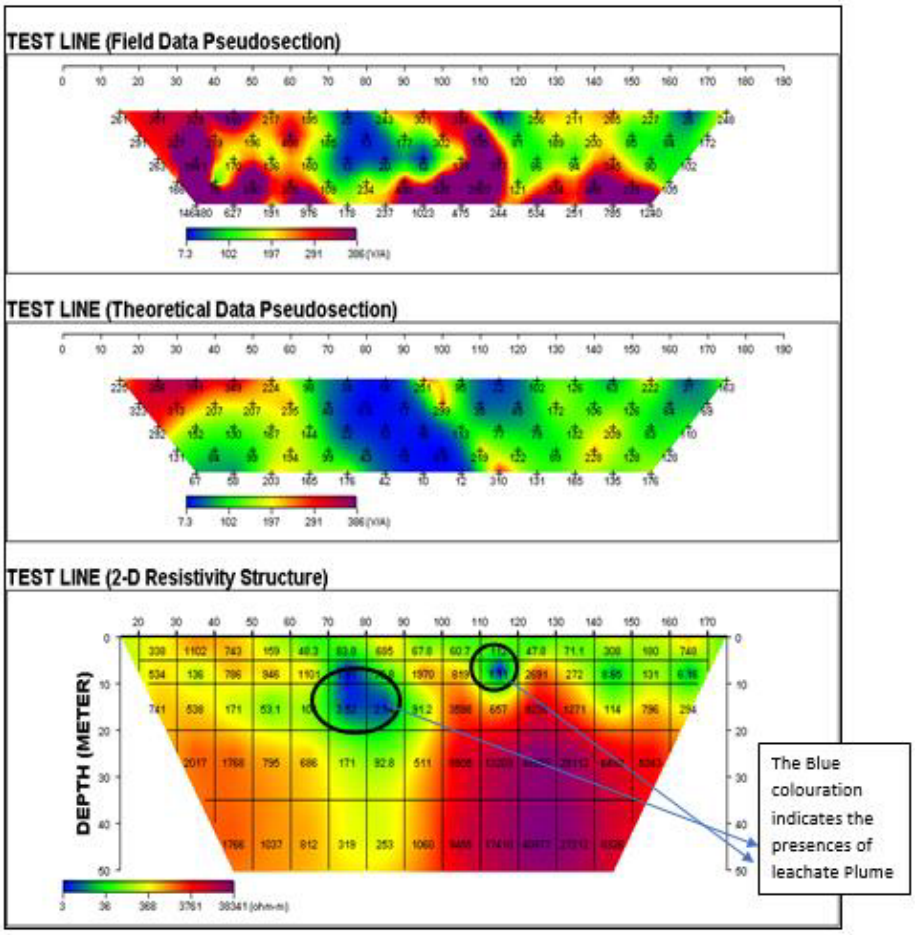

Figure 5. 2-D Resistivity structure based on FEM modeling of transverse 1 (2nd cemetery)

$$\rho_d = \frac{G_S}{1+e}\rho_w \quad (16)$$

$$e = G_s(1+w)\frac{\rho_w}{\rho} - 1 \quad (17)$$

$$S = \frac{wG_S}{e} \quad (18)$$

$$n = \frac{e}{1+e} \quad (19)$$

$$\gamma = \rho g \quad (20)$$

Where:

ρ	bulk density of soil in g/cm^3
ρ_d	dry density of soil in g/cm^3
ρ_w	density of water, taken as 1.0 g/cm^3
G_s	specific gravity of soil
w	moisture content in %
e	void ratio
S	degree of saturation in %
g	acceleration due to gravity, taken as 9.81 m/s^2
γ	Unit weight of soil in kN/m^2

Results and Discussion

The results of this study provide valuable insights into the vulnerability of the aquifer system to leachate contamination from cemetery activities in the study area.

Geotechnical Properties

Table 1 summarizes the geotechnical characteristics examined for the topsoil. The natural moisture content (NMC) ranges from 4.76% at 0m and 1m depth in BH3 to a maximum value of 56.77% at 3m depth in BH5, showing an increase with depth. Despite the majority of samples displaying low moisture content, with a mean value of 18.46 ± 4.33%, there is an observed trend of increasing moisture content with depth.

Dry density and bulk density values also increased with depth mirroring the pattern of natural moisture content. For example, bulk density varied from 1.62gcm^{-3} to 1.98gcm^{-3}, while dry density ranged from 1.04gcm^{-3} to 1.88gcm^{-3}. Notably, the density values from BH5 were lower than those from BH1, BH2, BH3, and BH4, indicating a strong water-holding capacity in the soil of this area, consistent with the high moisture content readings in BH5.

Porosity values for BH1, BH2, BH3, and BH4 ranged between 28.55% and 46.43%, while BH5 exhibited a higher range between 49.66% and 58.72%. In the particle size distribution study at a maximum depth of 3m, most soil samples contained less than 10% fines, which decreased with depth, and more than 80% sand. This aligns with the coefficient of uniformity findings, indicating that the topsoil has a very low level and was less than 8 for the majority of the examined soil samples.

Table 1. Descriptive statistics of topsoil geotechnical properties

Parameter	N	Min	Max	Mean
Specific Gravity	15	2.44	2.72	2.66 ± 0.13
Moisture Content	15	4.76	56.77	18.46 ± 4.33
Permeability	15	1.3E-4	4.7E-4	2.78E-4 ± 1.086E-4
Coefficient of Uniformity	15	1.33	12.65	4.022 ± 2.992
Porosity	15	28.55	58.72	37.09 ± 7.99
Void Ratio	15	0.37	1.78	0.55 ± 0.31
Bulk Density	15	1.62	1.98	2.03 ± 0.209
Dry Density	15	1.04	1.88	1.88 ± 0.354

Dipole-Dipole Investigation

Figure 4 provides a Google Earth image of second cemetery displaying the two transverse lines used for resistivity measurements. Resistivity data from transverse 1 is presented in Tables 2a and 2b, with the corresponding 2-D dipole-dipole profile maps in Figures 6 and 7. Similarly, resistivity data for transverse 2 is outlined in Table 3, and the corresponding 2-D dipole-dipole profile maps are depicted in Figures 8 and 9.

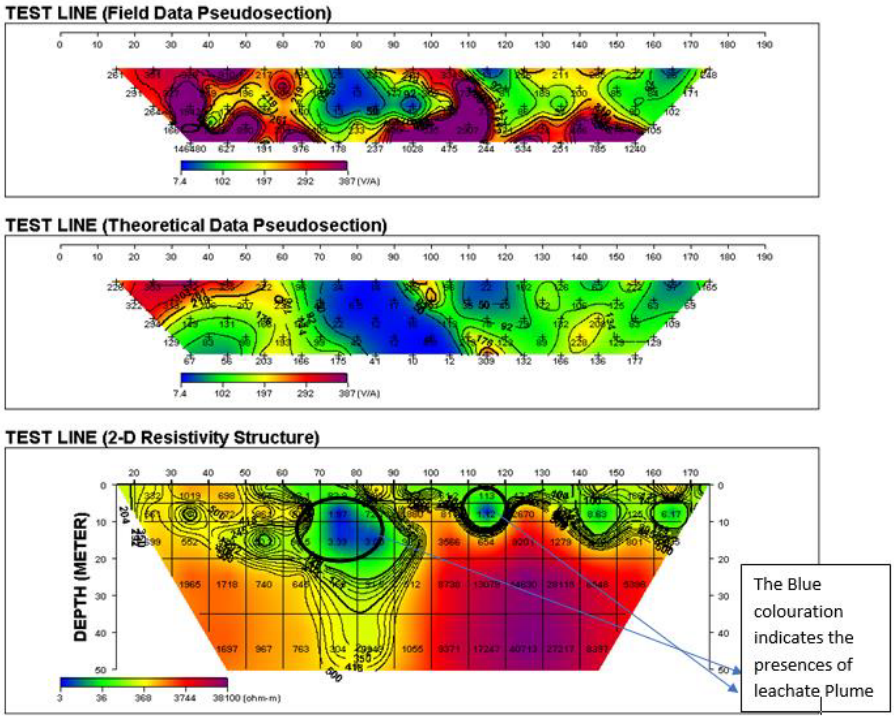

Figure 6. 2-D Resistivity structure with contours based on FEM modeling of transverse 1 (2nd Cemetery)

Table 2a. Dipole-Dipole data of transverse 1 obtained from the field (2nd Cemetery)

Electrode position				**Geometric**	**Resistance**	**Apparent Resistivity**
C1	C2	P1	P2	Factor	Ω	Ωm
0	10	20	30	188.52	1.386	261.28872
		30	40	754.08	0.386	291.07488
		40	50	1885.2	0.14	263.928
		50	60	3770.4	0.044	165.8976
		60	70	6598.2	22.2	146480.04
10	20	30	40	188.52	1.862	351.02424
		40	50	754.08	0.434	327.27072
		50	60	1885.2	1.03	1941.756
		60	70	3770.4	0.02	75.408
		70	80	6598.2	0.095	626.829
20	30	40	50	188.52	1.744	328.77888
		50	60	754.08	0.29	218.6832
		60	70	1885.2	0.09	169.668
		70	80	3770.4	0.236	889.8144
		80	90	6598.2	0.029	191.3478
30	40	50	60	188.52	4.83	910.5516
		60	70	754.08	0.26	196.0608
		70	80	1885.2	0.072	135.7344
		80	90	3770.4	0.081	305.4024
		90	100	6598.2	0.148	976.5336
40	50	60	70	188.52	1.153	217.36356
		70	80	754.08	0.541	407.95728
		80	90	1885.2	0.085	160.242
		90	100	3770.4	0.029	109.3416
		100	110	6598.2	0.027	178.1514
50	60	70	80	188.52	1.035	195.1182
		80	90	754.08	0.245	184.7496
		90	100	1885.2	0.007	13.1964
		100	110	3770.4	0.062	233.7648
		110	120	6598.2	0.036	237.5352
60	70	80	90	188.52	0.136	25.63872
		90	100	754.08	0.018	13.57344
		100	110	1885.2	0.011	20.7372

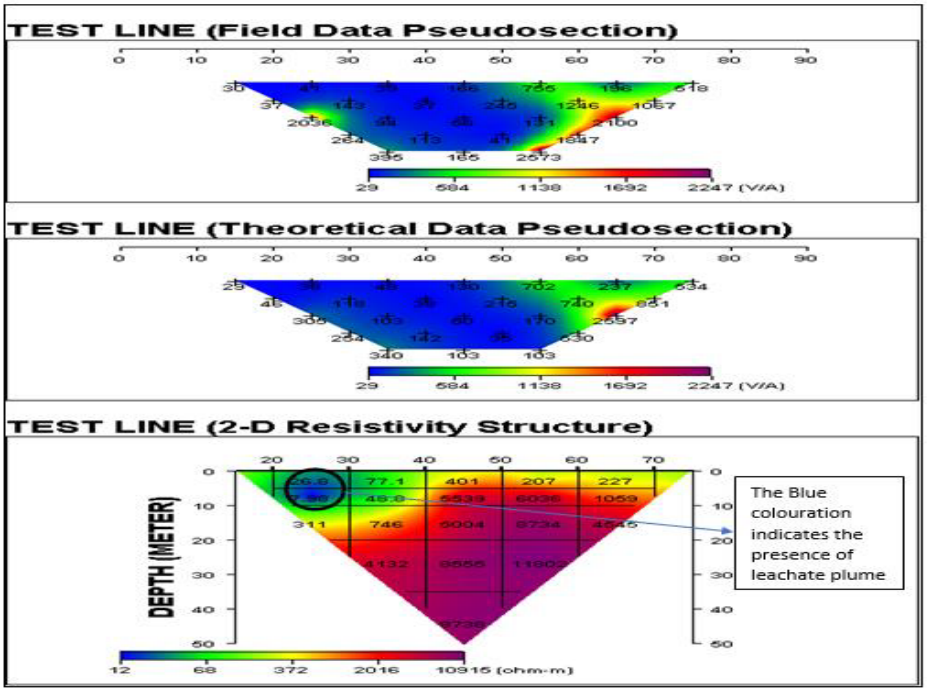

Figure 7. 2-D Resistivity structure based on FEM modeling of transverse 2 (2nd cemetery)

Table 2b. Dipole-Dipole data of transverse 1 obtained from the field (2nd Cemetery)

Electrode position				Geometric	Resistance	Apparent Resistivity
C1	C2	P1	P2	Factor	Ω	Ωm
		110	120	3770.4	0.106	399.6624
		120	130	6598.2	0.155	1022.721
70	80	90	100	188.52	1.288	242.81376
		100	110	754.08	0.235	177.2088
		110	120	1885.2	0.007	13.1964
		120	130	3770.4	0.142	535.3968
		130	140	6598.2	0.072	475.0704
80	90	100	110	188.52	1.597	301.06644
		110	120	754.08	0.401	302.38608
		120	130	1885.2	0.074	139.5048
		130	140	3770.4	0.771	2906.9784
		140	150	6598.2	0.037	244.1334
90	100	110	120	188.52	1.772	334.05744
		120	130	754.08	0.975	735.228
		130	140	1885.2	0.2	377.04
		140	150	3770.4	0.032	120.6528
		150	160	6598.2	0.081	534.4542
100	110	120	130	188.52	0.063	11.87676
		130	140	754.08	0.108	81.44064
		140	150	1885.2	0.046	86.7192
		150	160	3770.4	0.086	324.2544
		160	170	6598.2	0.038	250.7316
110	120	130	140	188.52	1.36	256.3872
		140	150	754.08	0.251	189.27408
		150	160	1885.2	0.05	94.26
		160	170	3770.4	0.129	486.3816
		170	180	6598.2	0.119	785.1858
120	130	140	150	188.52	1.12	211.1424
		150	160	754.08	0.266	200.58528
		160	170	1885.2	0.13	245.076
		170	180	3770.4	0.073	275.2392
		180	190	6598.2	0.188	1240.4616
130	140	150	160	188.52	1.408	265.43616
		160	170	754.08	0.113	85.21104
		170	180	1885.2	0.048	90.4896
		180	190	3770.4	0.028	105.5712
		190	200	6598.2	0.106	699.4092
140	150	160	170	188.52	1.206	227.35512

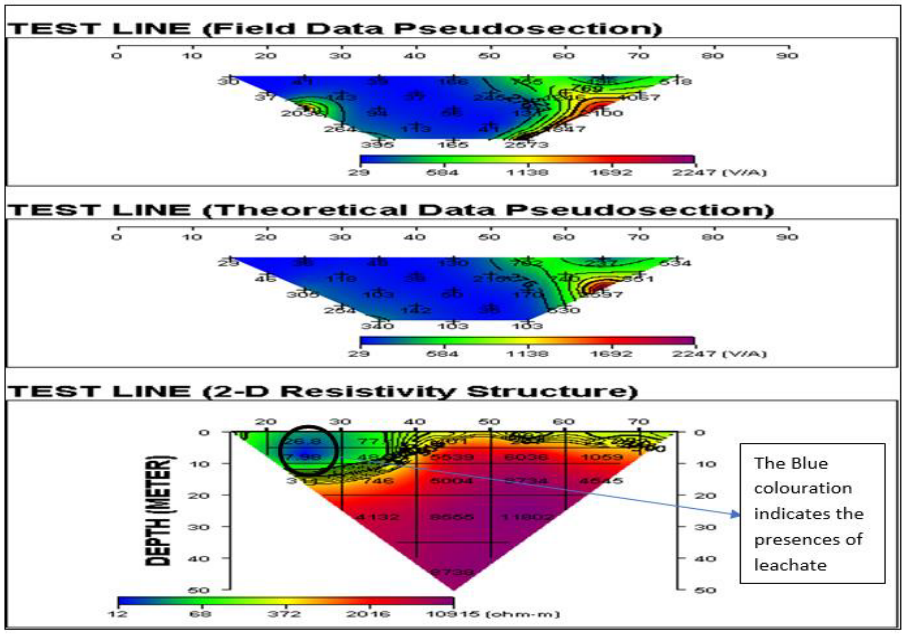

Figure 8. 2-D Resistivity structure with contours based on FEM modeling of transverse 2 (2nd Cemetery)

Table 3. Dipole-Dipole data of transverse 2 obtained from the field (2nd Cemetery)

Electrode position				**Geometric**	**Resistance**	**Apparent**
C1	C2	P1	P2	Factor	Ω	**ResistivityΩm**
0	10	20	30	188.52	0.16	30.1632
		30	40	754.08	0.05	37.704
		40	50	1885.2	1.08	2036.016
		50	60	3770.4	0.07	263.928
		60	70	6598.2	0.06	395.892
10	20	30	40	188.52	0.22	41.4744
		40	50	754.08	0.19	143.2752
		50	60	1885.2	0.05	94.26
		60	70	3770.4	0.03	113.112
		70	80	6598.2	0.025	164.955
20	30	40	50	188.52	0.21	39.5892
		50	60	754.08	0.05	37.704
		60	70	1885.2	0.03	56.556
		70	80	3770.4	0.011	41.4744
		80	90	6598.2	0.39	2573.298
30	40	50	60	188.52	0.24	45.2448
		60	70	754.08	0.22	165.8976
		70	80	1885.2	0.13	245.076
		80	90	3770.4	0.035	131.964
		90	100	6598.2	0.28	1847.496
40	50	60	70	188.52	1.609	303.32868
		70	80	754.08	1.001	754.83408
		80	90	1885.2	0.661	1246.1172
		90	100	3770.4	0.557	2100.1128
50	60	70	80	188.52	1.04	196.0608
		80	90	754.08	1.416	1067.77728
		90	100	1885.2	0.698	1315.8696
60	70	80	90	188.52	2.75	518.43
		90	100	754.08	0.077	58.06416
70	80	90	100	188.52	0.324	61.08048

Figure 9: Google earth image of 2nd cemetery showing the established points for VES analysis

Observations from the profile maps indicate that the surface of the study area has resistivity ranged of 34Ωm to 180Ωm which increases with depth. Leachate plumes, observed at depths of 5 to 20 meters, have traveled horizontally approximately 70m to 120 meters in a northeastern (NE) direction. The topsoil in this horizontal direction was observed to be contaminated with necroleachate from cemetery activities. For transverse 2, the topsoil resistivity data which ranged from 48.8Ωm to 77.1Ωm also increases with depth. Necroleachate was detected at depth of 0 to 10 meters, having traveled horizontally 20m to 30 meters with a resistivity range of 7.98Ωm to 26.8Ωm.

The 2-D dipole-dipole profile map confirms the northeast (NE) direction of leachate movement. The outcome indicates the presence of a necroleachate plume at depths of 5 to 20 meters and 0 to 10 meters as illustrated in Figures 5, 6, 7, and 8. Both traverses pinpoint the cemetery operations as the source of the leachate plume, specifically exposing the activities at a depth of 5 to 20 meters for traverse 1 and the presence of the plume from the surface to a depth of 0 to 10 meters for traverse 2 indicate significant subsurface contamination. Necroleachate resulting from the decomposition of dead bodies contains heavy metals and other toxic substances due to the decay of coffin material (Spongberg & Becks, 2000; Jonker & Olivier, 2012). Traverse 1 exposes the actual activities at a depth of 5 to 20 meters, while traverse 2 indicates the presence of the leachate plume from the surface (topsoil) to a depth of 0 to 10 meters.

Vertical Electrical Sounding

To gain insights into the vulnerability of the aquifer around second cemetery to necroleachate contamination and determine the geoelectric layer that characterizes the aquifer, 1-D geophysical technique known as Vertical Electrical Sounding (VES) was employed. The technique is valuable for estimating the thickness of loose horizontal overburden over hard rocks in river valleys and groundwater projects. The Google Earth image in Figure 9 displays second cemetery and the selected VES locations while Tables S1a to S8a present the VES data acquired from the field survey. From the VES data, it was observed that resistivity values increase with depth. The geoelectric resistivity model parameters presented in Table 4 were estimated using the VES field data while the summary of the computed electrical properties of the aquifer is presented in Table 5. In addition, the lithology of the aquifer and the layer inversion model based on the VES is presented in Tables S1b to S8b and Figures 10 to 17 respectively.

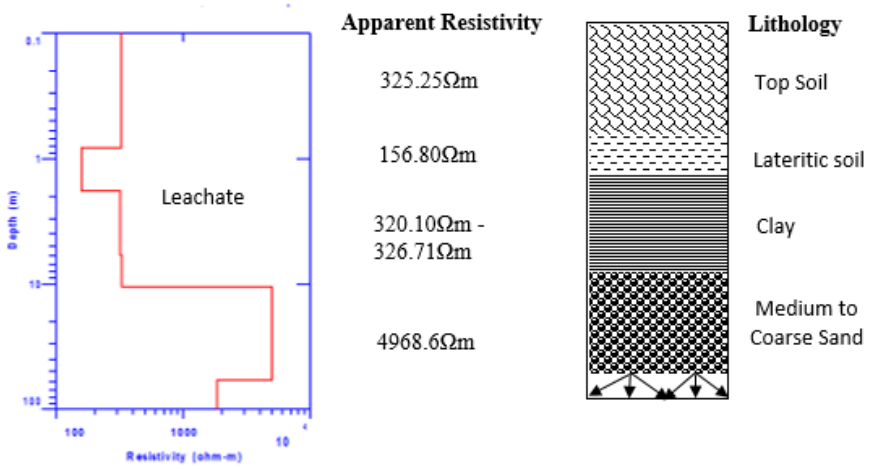

Figure 10. Layered Inversion Model and Lithology of VES point 1

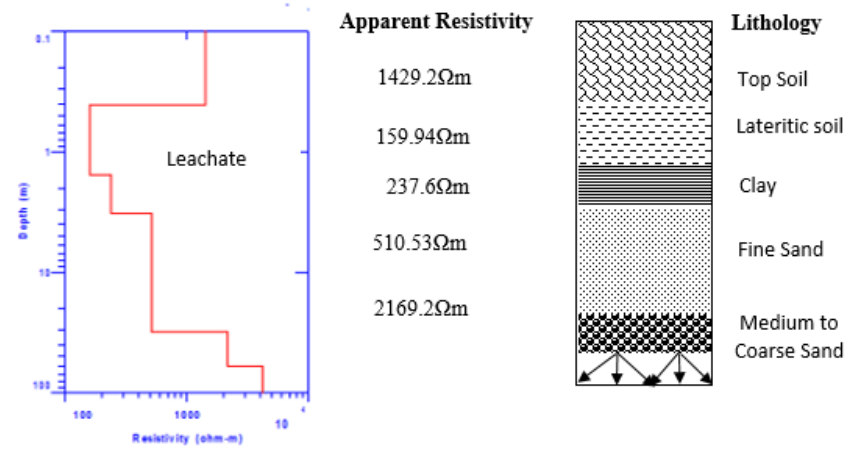

Figure 11. Layered Inversion Model and Lithology of VES point 2

Table 4. Summary of VES interpretation results

Number of Transverse points	Apparent Resistivity	Thickness	Longitudinal conductance (S, Ω^{-1})	Transverse Resistance (TR, Ωm^2)	Coordinates points
VES 1	325.25	0.8144	0.00250392	264.8836	**Coordinate: N 06° 20.436' E 005° 36.517' Elevation: 156m**
	156.80	0.9907	0.00631824	155.34176	
	320.10	4.0772	0.01273727	1305.11172	
	326.71	4.6280	0.014165468	1512.01388	
	4968.6	47.489	0.009557823	235953.845	
VES 2	1429.2	0.4093	0.000286384	584.97156	**Coordinates: N 06° 20.458' E005° 36.466' Elevation: 91m**
	159.94	1.1307	0.007069526	180.844158	
	237.63	1.6857	0.007093801	400.572891	
	510.53	28.190	0.055217127	14391.8407	
	2169.2	28.717	0.013238521	62292.9164	
VES 3	571.66	0.2999	0.000524613	171.440834	**Coordinate: N 06° 20.402', E 005° 36.406', Elevation: 80m**
	76.303	1.1437	0.014988926	87.2677411	
	65.864	3.6249	0.055036135	238.7504136	
	204.63	3.0164	0.014740752	617.245932	
	3833.5	44.318	0.011560715	169893.053	
VES 4	173.73	0.5259	0.003027111	91.364607	**Coordinate N 06°20.458', E 005°36.411' Elevation: 80m**
	15.394	0.6334	0.041145901	9.7505596	
	911.33	4.1935	0.004601516	3821.66235	
	339.84	7.1136	0.020932203	2417.48582	
	515.92	8.4352	0.016349822	4351.88838	
VES 5	101.53	0.5977	0.00588693	60.684481	**Coordinate: N 06° 20.427' E 005° 36.435' Elevation: 87m**
	25.138	1.1042	0.043925531	27.7573796	
	6329.2	12.602	0.001991089	79760.5784	
	543.87	31.752	0.058381599	17268.96024	
VES 6	62.530	1.4313	0.022889813	89.499189	**Coordinate: N 06° 20.407' E 005° 36.477' Elevation: 77m**
	27.522	2.6639	0.096791658	73.3158558	
	3373.8	14.838	0.004398008	50060.4444	
	689.79	32.032	0.046437322	22095.35328	
VES 7	597.75	0.4689	0.000784442	280.284975	**Coordinate N 06° 20.294', E 05° 36.544', Elevation: 85m**
	118.20	1.8959	0.016039763	224.09538	
	84.635	5.5560	0.0656466	470.23206	
	189.14	8.3891	0.044353918	1586.714374	
	933.02	38.493	0.04125635	35914.73886	
VES 8	544.91	0.3451	0.000633316	188.048441	**Coordinate: N 06° 20.502, E 005° 36.551' Elevation: 94m**
	43.205	0.8516	0.019710682	36.793378	
	338.78	3.2896	0.009710136	1114.450688	
	71.048	2.4381	0.034316237	173.2221288	
	9954.3	32.021	0.003216801	318746.6403	

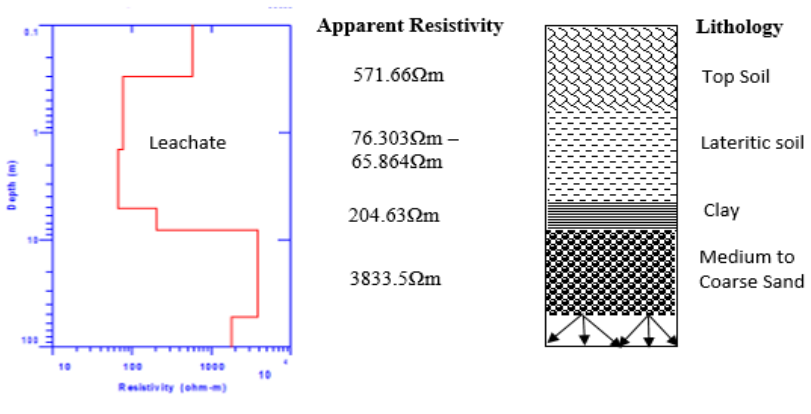

Figure 12. Layered Inversion Model and Lithology of VES point 3

Table 5. Summary of Electrical Properties of Aquifer

Sounding points	Mean Apparent Resistivity (Ωm)	Mean Thickness (m)	Conductivity (**δ**, Ωm^{-1})	Longitudinal conductance (**S**, Ω^{-1})	Transverse Resistance (**TR**, Ωm^2)	Hydraulic Conductivity (**K**)	Transmissivity (Tr, m^2/day)
VES 1	1219.49	11.599	0.0008200	0.009511	14144.8645	0.51069	5.92349331
VES 2	901.3	12.026	0.001109	0.013343	10839.0338	0.67709	8.14268434
VES 3	950.39	10.48	0.001052	0.011027	9960.0872	0.64441	6.7534168
VES 4	1242.78	7.602	0.0008046	0.006117	9447.61356	0.50176	3.81437952
VES 5	1749.93	11.5139	0.0005714	0.006580	20148.5190	0.36463	4.198313357
VES 6	1038.41	12.741	0.0009630	0.012270	13230.3818	0.5933	7.5592353
VES 7	384.55	10.9605	0.0026004	0.028502	4214.86027	1.49871	16.42661096
VES 8	2190.45	7.7891	0.0004565	0.003556	17061.6341	0.29572	2.303392652

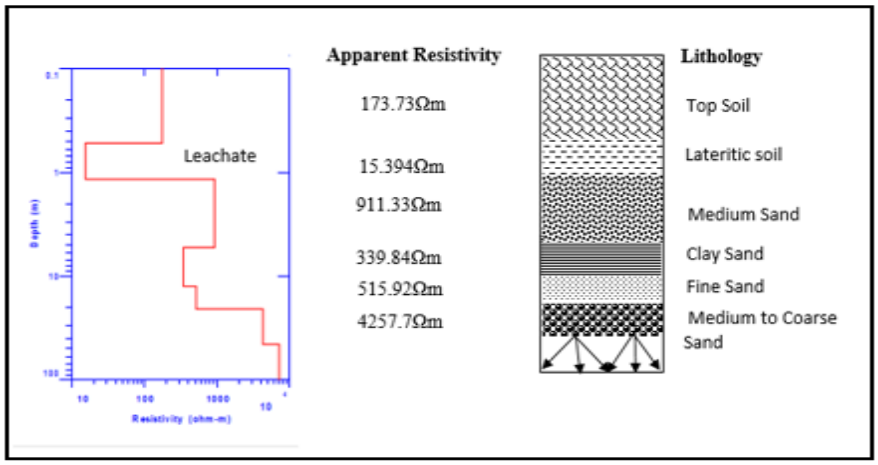

Figure 13. Layered Inversion Model and Lithology of VES point 4

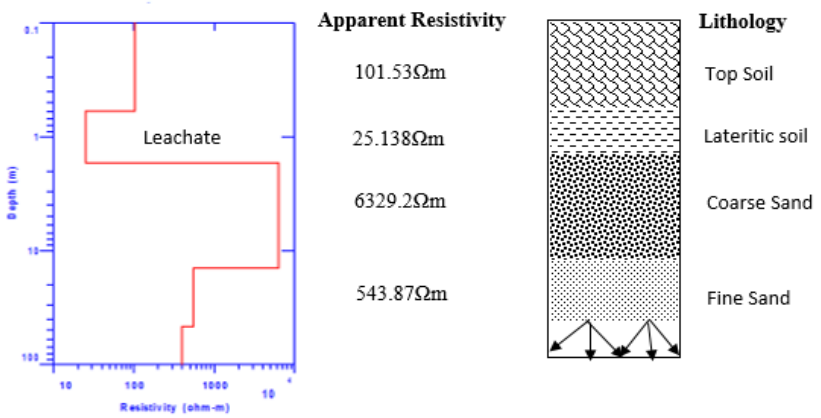

Figure 14. Layered Inversion Model and Lithology of VES point 5

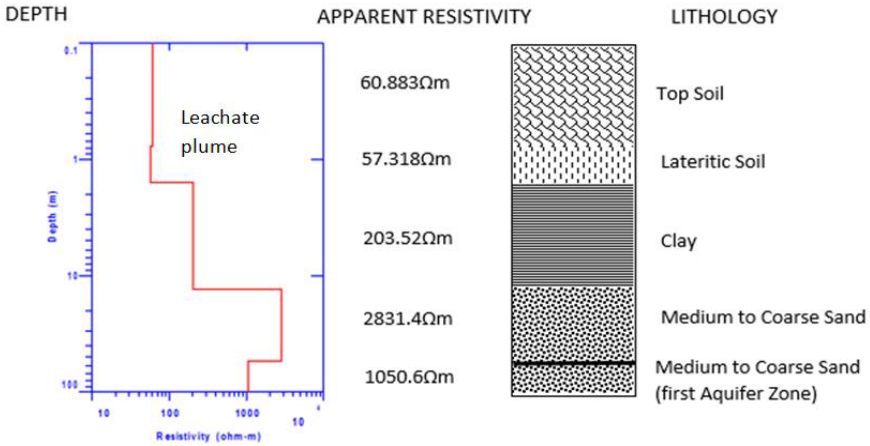

Figure 15. Layered Inversion Model and Lithology of VES point 6

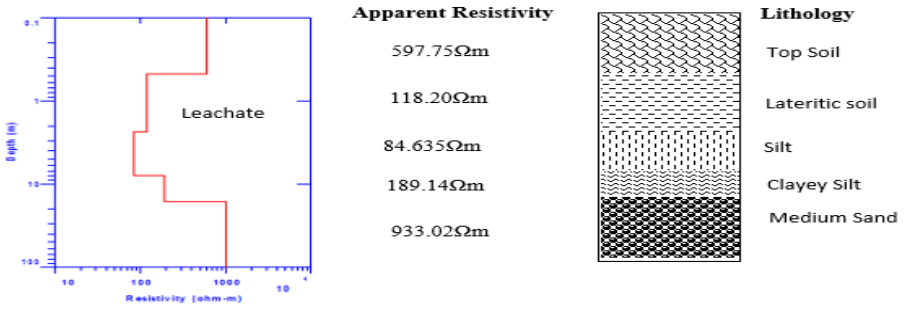

Figure 16. Layered Inversion Model and Lithology of VES point 7

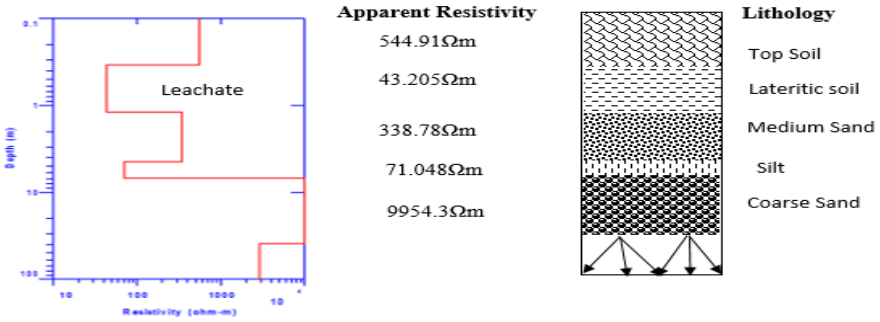

Figure 17. Layered Inversion Model and Lithology of VES point 8

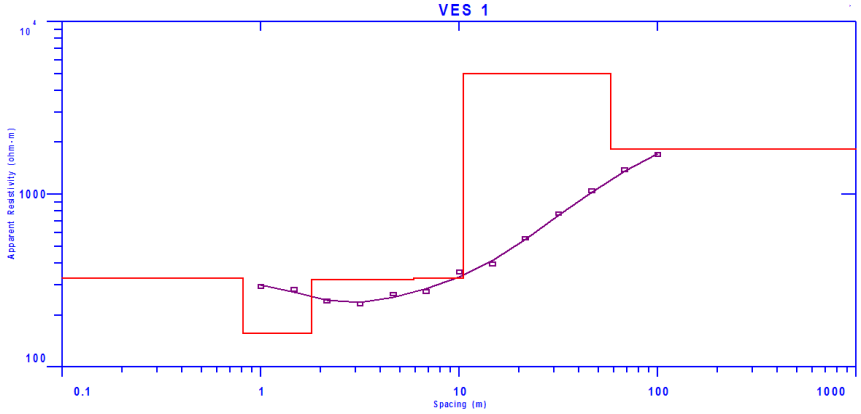

Figure 18. Typical hydrogeophysical sounding curve of VES 1

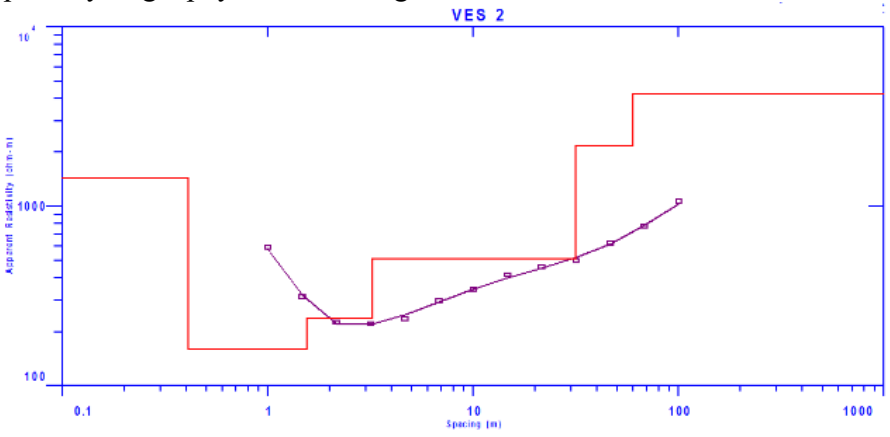

Figure 19. Typical hydrogeophysical sounding curve of VES 2

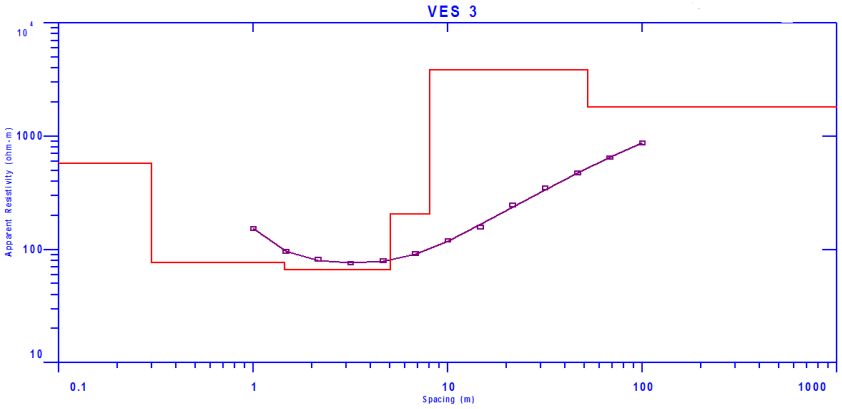

Figure 20. Typical hydrogeophysical sounding curve of VES 3

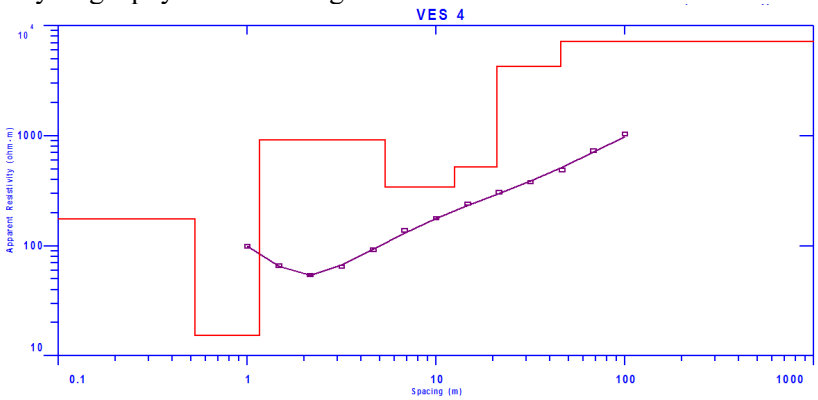

Figure 21. Typical hydrogeophysical sounding curve of VES 4

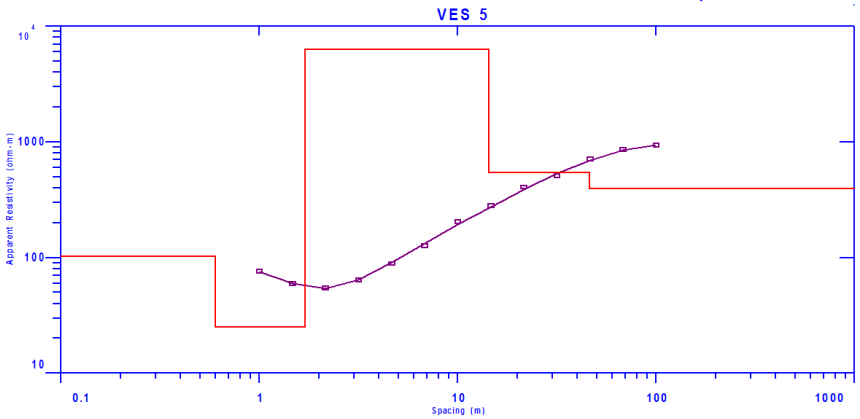

Figure 22. Typical hydro-geophysical sounding curve of VES 5

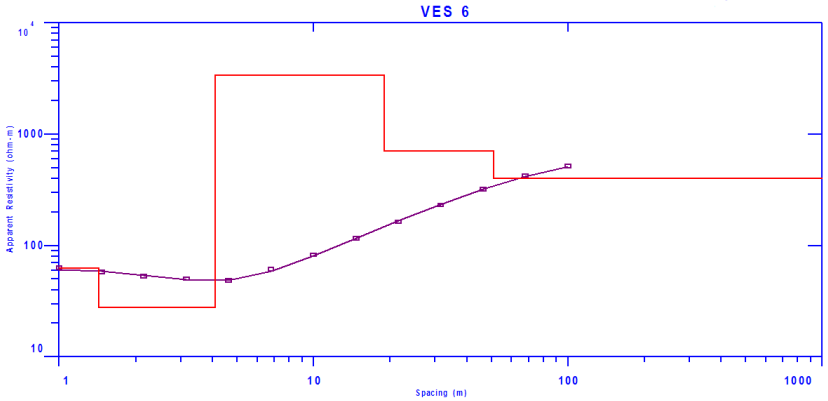

Figure 23. Typical hydro-geophysical sounding curve of VES 6

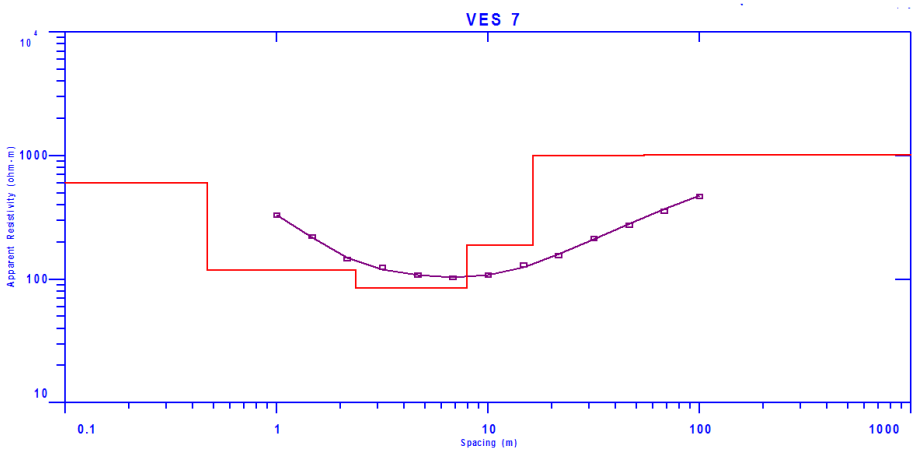

Figure 24. Typical hydrogeophysical sounding curve of VES 7

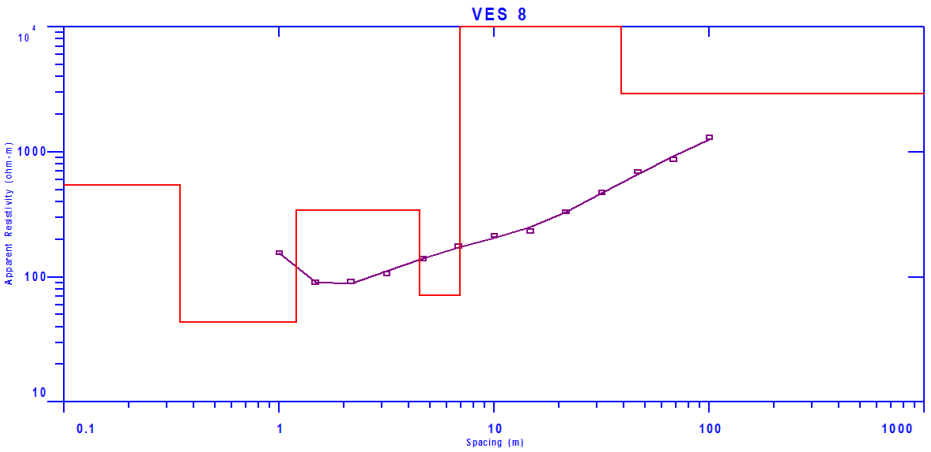

Figure 25. Typical hydrogeophysical sounding curve of VES 8

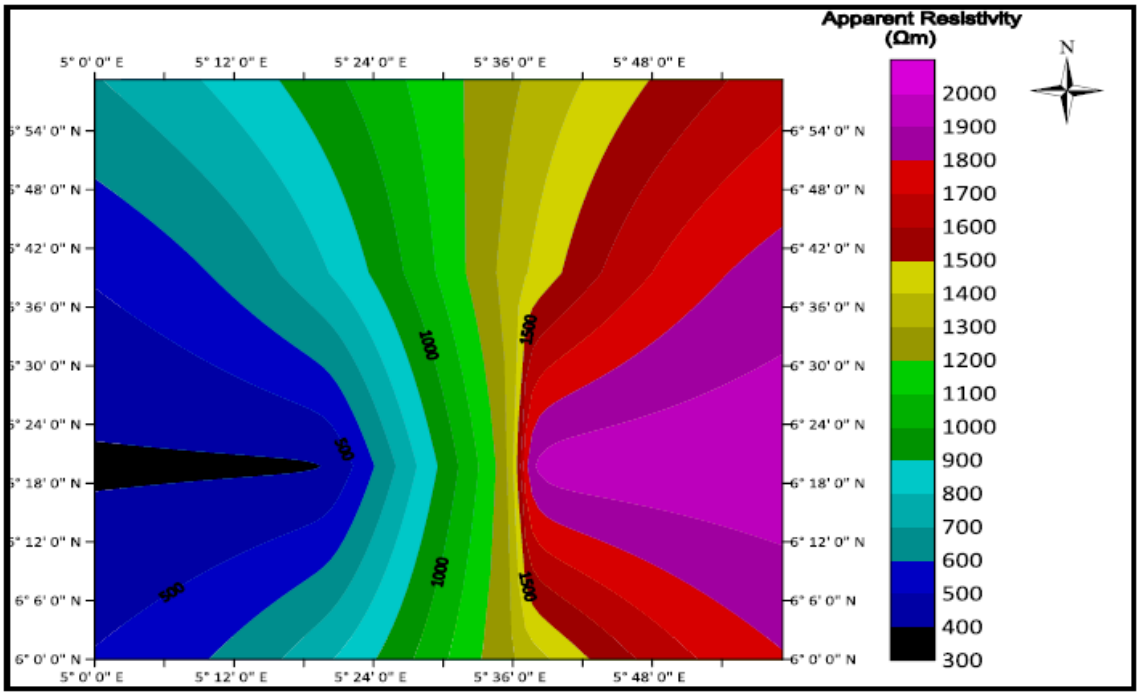

Figure 26. Apparent Resistivity contour map of second cemetery

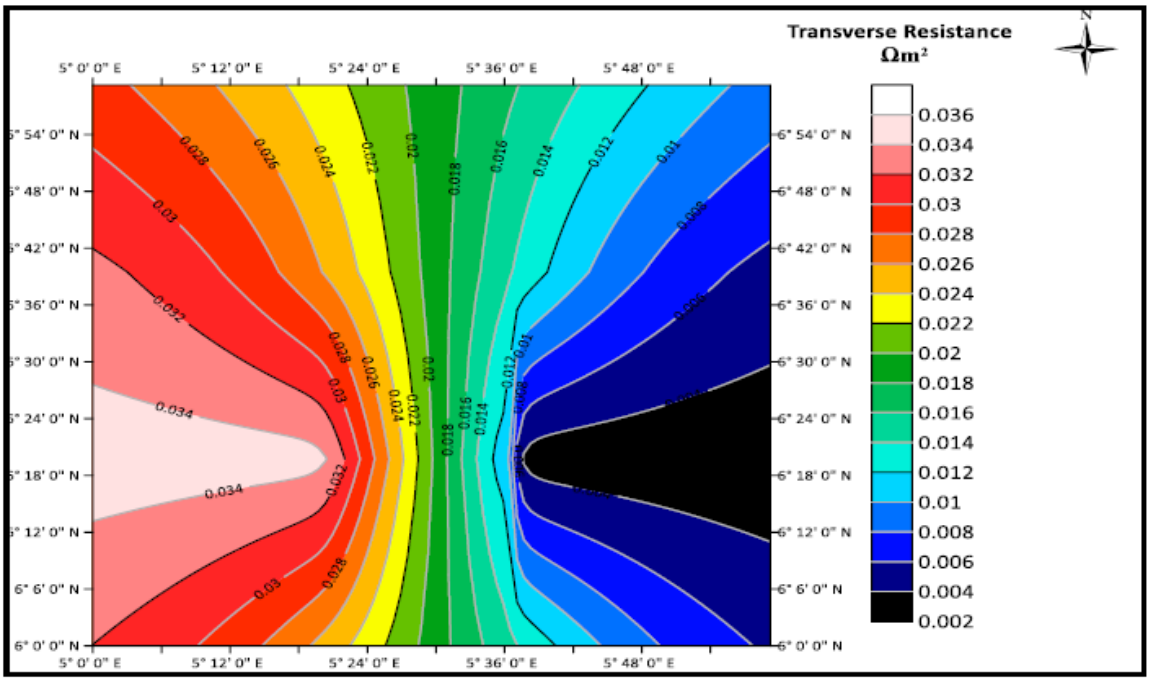

Figure 27. Transverse Resistance contour map of second cemetery

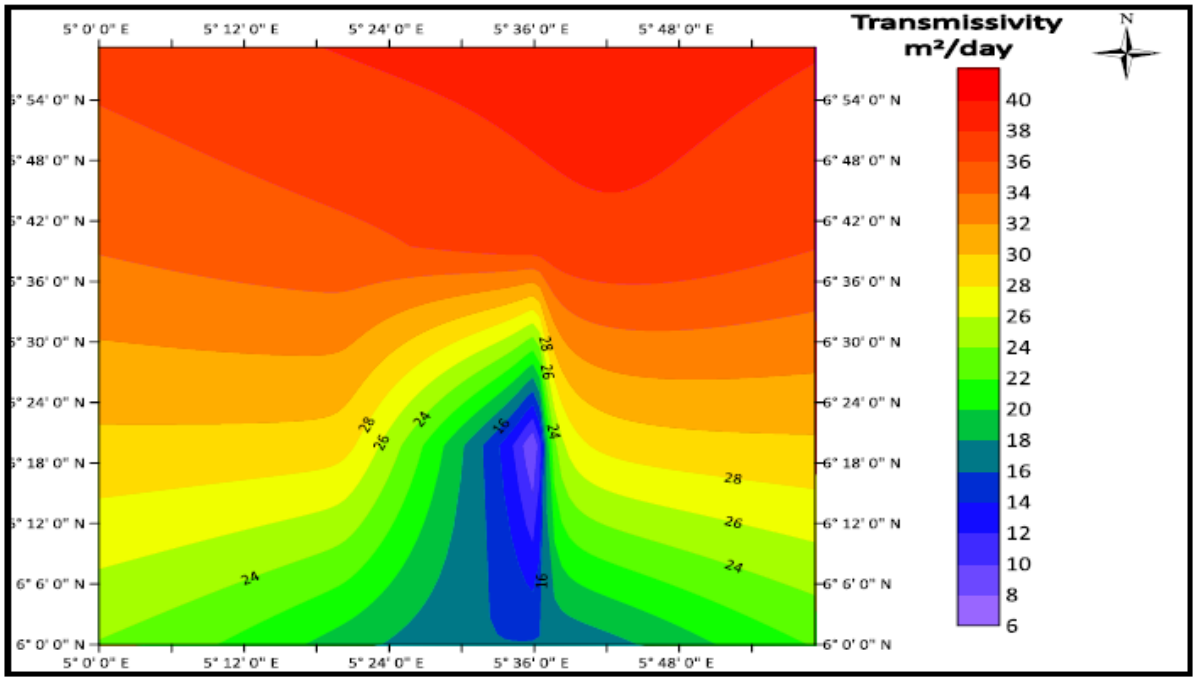

Figure 28. Transmissivity contour map of the study area.

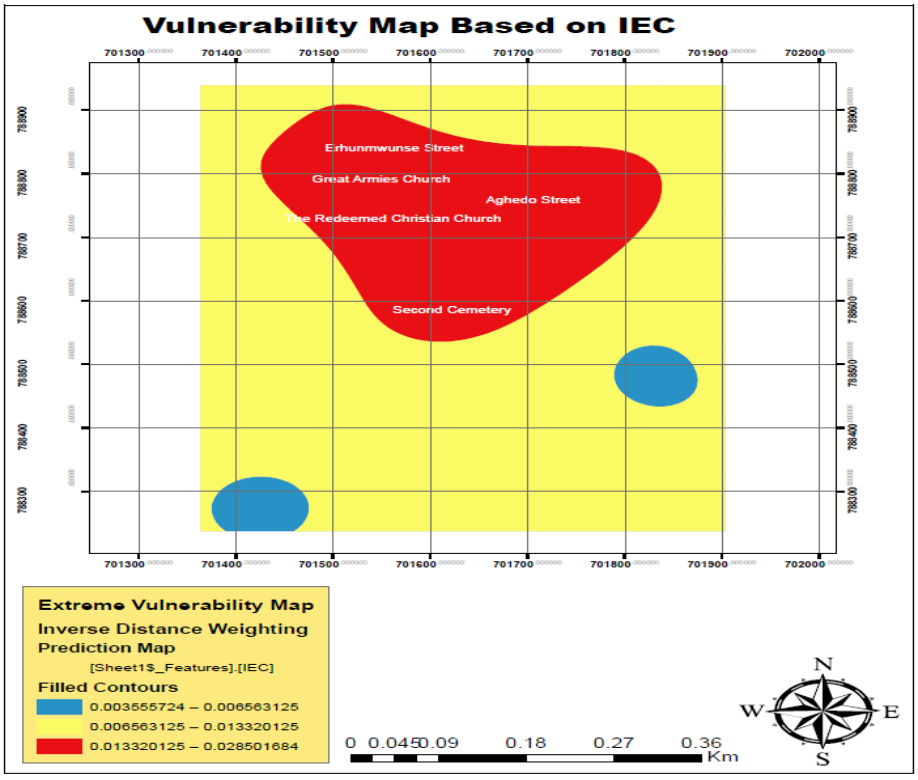

Figure 29. Vulnerability map based on Integrated Electrical Conductivity (IEC)

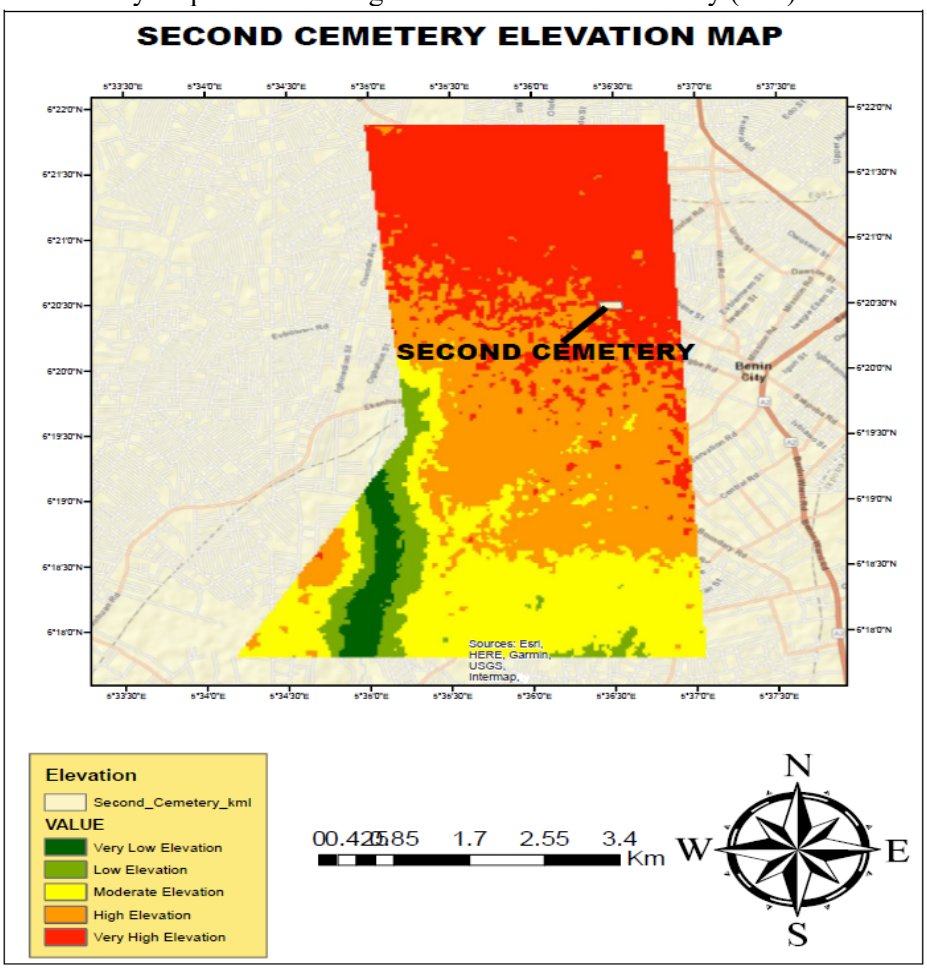

Figure 30. Second cemetery elevation map

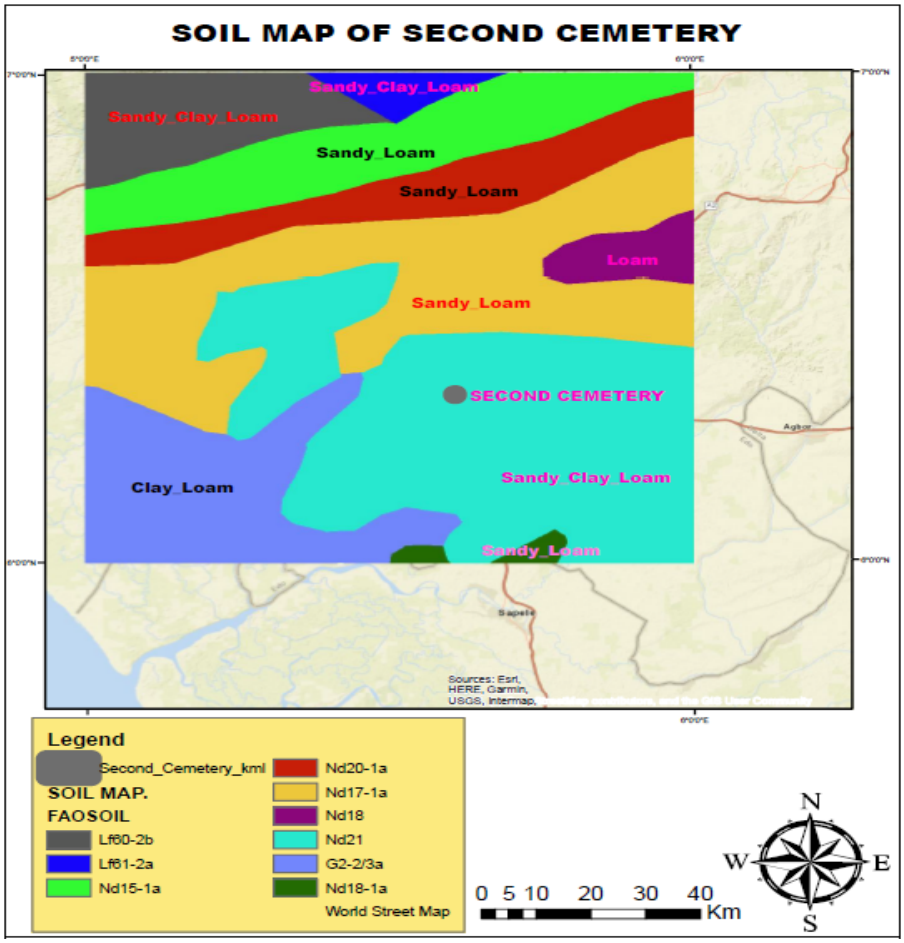

Figure 31. Second cemetery soil map

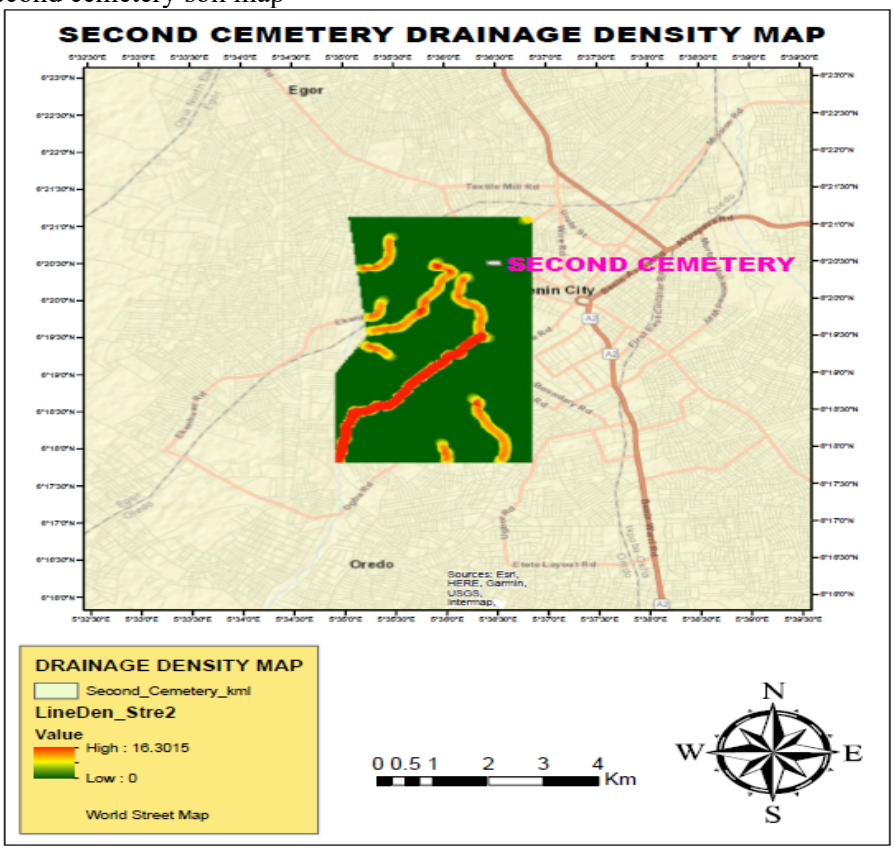

Figure 32. Second cemetery drainage density map

Figure 33. Second cemetery, Benin City

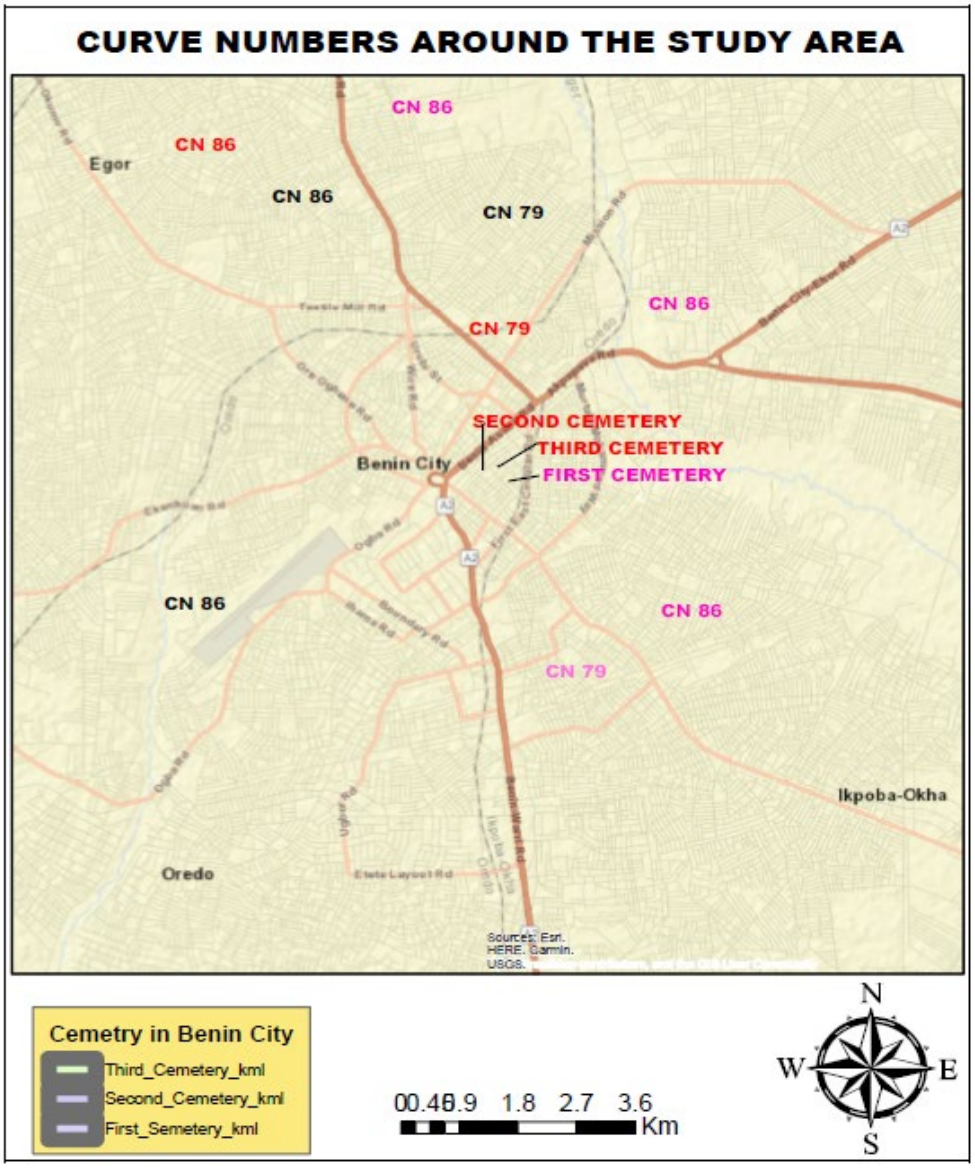

Figure 34. curve number around the vicinity of cemetery in Benin City

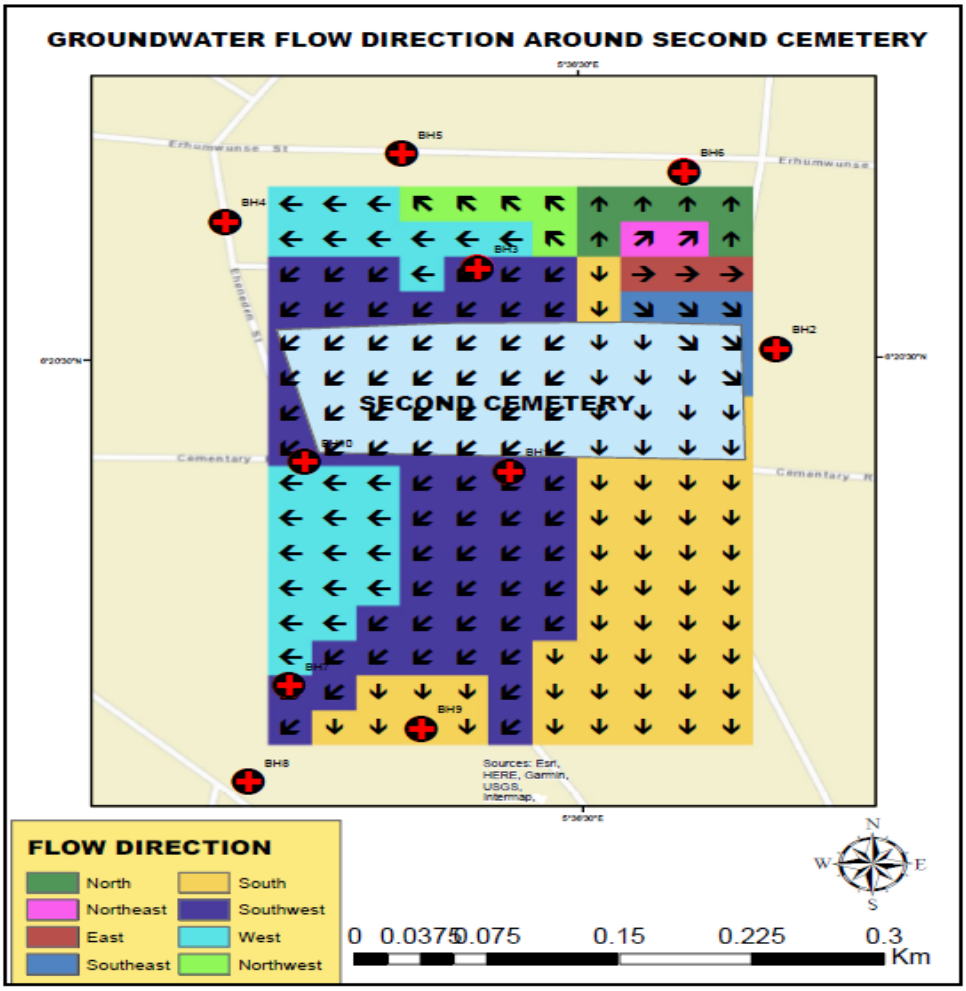

Figure 35. Flow of groundwater around second cemetery

The VES summary result is presented as follows

1. **VES at Location S1:** The modeling revealed six geoelectric layers, including clay and sand, with resistivity ranging from 325.25Ωm to 4968.6Ωm. The average thickness of the clay layer was 4.6280m, and the sand layer had a thickness of 4968m, extending to an undetermined depth.
2. **VES at Location S2:** Similar to S1, this VES showed six geoelectric layers, with clay and sand, resistivity ranging from 159.94Ωm to 2169.2Ωm. The average thickness of the clay layer was 1.6857m, and the sand layer varied from 28.19m to 28.717m, extending to an undetermined depth.
3. **VES at Location S3:** Six geoelectric layers were identified, with clay and sand, resistivity ranging from 65.864Ωm to 3833.5Ωm. The average thickness of the clay layer was 3.0164m, and the sand layer had a thickness of 44.318m, extending to an undetermined depth.
4. **VES at Location S4:** This VES revealed six geoelectric layers, including clay and sand, resistivity ranging from 15.394Ωm to 7144.5Ωm. The average thickness of the clay layer was 7.1136m, and the sand layer varied from 8.4352m to 24.709m, extending to an undetermined depth.
5. **VES at Location S5:** Modeling indicated five geoelectric layers, with the third and fourth layers being sand. Resistivity ranged from 25.138Ωm to 6329.2Ωm. The thickness of the sand layers varied from 12.602m to 31.752m, extending to a depth of 46.056m.
6. **VES at Location S6:** Similar to S5, this VES showed five geoelectric layers, with the third and fourth layers being sand. Resistivity ranged from 7.522Ωm to 689.79Ωm. The thickness of the sand layers varied from 14.838m to 32.032m, extending to a depth of 50.966m.
7. **VES at Location S7:** Six geoelectric layers were identified, with clay and sand, resistivity ranging from 597.75Ωm to 933.02Ωm. The average thickness of the clay layer was 8.3891m, and the sand layer had a thickness of 38.493m, extending to an undetermined depth.

8. **VES at Location S8:** This VES revealed six geoelectric layers, with the fifth and sixth layers being sand. Resistivity ranged from 43.205Ωm to 2905.2Ωm. The thickness of the sand layers was 32.021m, extending to an undetermined depth.

The typical hydro-geophysical sounding curves of the VES are presented in Figures 18 to 25. The presence of clay layers just below the topsoil suggests effective prevention of leachate penetration into the subsurface. The clay acts as both a seal and a filter for leachate resulting from decomposition, potentially containing pollution to the topsoil. These findings contribute to the understanding of the aquifer's vulnerability to necroleachate contamination, indicating the importance of the geological composition in preventing downward leachate migration.

Geophysical Interpretation and Maps

The apparent resistivity contour map, illustrated in Figure 26, serves as a visual representation of the spatial distribution of apparent resistivity values across the study area. Contour lines connect points with similar resistivity values, highlighting variations and anomalies in subsurface resistivity. Analyzing this map provides insights into geological features, subsurface structures, and hydrogeological characteristics.

- ✓ High Apparent Resistivity: Indicates materials with low electrical conductivity, such as dry or compacted soil, clay, or bedrock. These materials impede electrical current flow, suggesting higher resistivity.
- ✓ Potential Porous or Fractured Media: Areas with high resistivity may signify porous or fractured formations, indicating lower water content or higher air-filled voids. Examples include sandy or gravely formations, fractured bedrock, or zones with low moisture content.

The Transverse Resistance Contour Map, depicted in Figure 27, is a valuable tool in groundwater studies, environmental investigations, geotechnical engineering, and mineral exploration. It provides insights into subsurface lithology, geological structures, groundwater flow patterns, and areas of interest.

- ✓ High Transverse Resistance: Corresponds to areas with higher resistivity, such as clay or bedrock, restricting electrical current flow.
- ✓ Low Transverse Resistance: Indicates zones of lower resistivity, suggesting sandy or water-bearing formations.

The Transmissivity Contour Map (Figure 28) offers information on areas with greater potential for groundwater flow and recharge. This map helps identify permeable aquifer layers and areas conducive to groundwater movement.

- ✓ High Transmissivity Zones: Associated with greater groundwater flow potential, indicating permeable and thicker aquifer layers.
- ✓ Low Transmissivity Areas: Suggest reduced groundwater flow, pointing to less permeable or thinner aquifer sections.

Alignment of transmissivity contours with topography or regional geological features provides insights into dominant flow pathways and potential groundwater discharge areas. These maps collectively contribute to a comprehensive understanding of subsurface conditions, aiding in effective groundwater management and environmental protection strategies.

Aquifer Vulnerability Assessment

The basic connection between an aquifer's sensitivity and electrical conductivity is based on the fundamental idea known as the clay content of the substance. Clay content affects electrical resistance or conductivity and is connected to soil hydraulic conductivities (Schenk et al., 2020; Simsek *et al*., 2006). In general, low hydraulic conductivities and high clay contents are correlated with low electrical resistivity's and high electrical conductivities (Sen et al., 1988). The aquifer vulnerability index (AVI), which is a widely used measure to determine how vulnerable an aquifer is to surface contamination, is like the notion of vulnerability assessment. With the unsaturated layers, this technique measures groundwater vulnerability. The aquifer's hydraulic resistance (C) was calculated using

$$C = \sum_{i=1}^{n} \frac{h_i}{k_i} \quad (21)$$

Where; k_i and h_i are the hydraulic conductivity and the thickness of the layer above the aquifer zone. The hydraulic conductivity (k_i) can be replaced by the electrical conductivity (δ_i) or the resistivity (ρ_i) to calculate the hydraulic resistance (C) which is called Integrated Electrical Conductivity, IEC (Intrinsic Electrical Conductivity) (Röttger *et al*., 2005) or a Geophysical Based Protection Index (GPI) as proposed by Casas et al. (2008). The IEC can be used to assess the aquifer vulnerability by measuring the conductivity of the unsaturated zone, which provides an indication of the ease with which contaminants can travel through the subsurface to reach the aquifer. This method relies on the principle that materials with higher clay content and lower hydraulic conductivity will have higher electrical conductivity, thus indicating a higher vulnerability to contamination.

$$IEC = \sum_{i=1}^{n} h_i . \frac{1}{\rho_i} \quad (22)$$

Equation (22) can be rewritten as;

$$IEC = \sum_{i=1}^{n} h_i . \delta_i \quad (23)$$

Where; $\delta_i = \frac{1}{\rho_i}$

From the inversion of resistivity sounding, the resistivity (i) and thickness (hi) of each layer above the aquifer were determined. The estimated IEC unit is either Siemens (S) or ohm^{-1} (1). For all levels above the groundwater table in the study region, the vulnerability index or integrated conductivity was determined. Table 6 presents the estimated IEC of the aquifer. The estimated IEC index indicates that the aquifer's vulnerability lies between 0.003556 and 0.028502S. The aquifer was determined to be extremely sensitive to contamination based on the vulnerability criteria shown in Table 7. A vulnerability map was created and presented in Figure 29 to show the precise locations in the research area that fall under this extremely risky region. Aquifer vulnerability issues are likely to affect places like Erhunmwunse Street, Great Armies Church, Aghedo Street, and Second Cemetery Road, according to the map.

Table 6. Estimated IEC of aquifer around second cemetery

VES Points	Mean Apparent Resistivity (Ωm)	Mean Thickness (m)	Conductivity (δ, Ωm^{-1})	Computed IEC (S)
VES 1	1219.49	11.599	0.0008200	0.009511
VES 2	901.3	12.026	0.001109	0.013337
VES 3	950.39	10.48	0.001052	0.011025
VES 4	1242.78	7.602	0.0008046	0.006117
VES 5	1749.93	11.5139	0.0005714	0.006579
VES 6	1038.41	12.741	0.0009630	0.01227
VES 7	384.55	10.9605	0.0026004	0.028502
VES 8	2190.45	7.7891	0.0004565	0.003556

Table 7. Vulnerability assessment criteria base on IEC method

Degree of vulnerability	Vulnerability index (mS)
Extremely High	<500
High	500-1000
Moderate	1000-2000
Low	2000-4000
Extremely Low	>4000

Table 8. Curve number value around the vicinity of cemetery in Benin City

S/N	Soil Codes	FAO Soil Code	Soil Type	HYDGRP	CN
1	Lf60-2b	1484	Sandy_Clay_Loam	C	86
2	Lf61-2a	1485	Sandy_Clay_Loam	C	86
3	Nd15-1a	1552	Sandy_Loam	C	86
4	Nd20-1a	1558	Sandy_Loam	B	79
5	Nd17-1a	1554	Sandy_Loam	B	79
6	Nd18	1555	Loam	C	86
7	Nd21	1559	Sandy_Clay_Loam	C	86
8	Ge-2/3a	1193	Clay_Loam	C	86
9	Nd18-1a	1556	Sandy_Loam	B	79

Table 9. FAO user soil table

SEQN	SNAM	NLAYERS	HYDGRP	SOL_ZMX	ANION_EXCL	SOL_CRK	TEXTURE
0	Sample-0	4	A	2032	0.5	0.5	LFS-LFS-S
1	Af14-3c-1	2	C	750	0.5	0.5	CLAY_LOAM
2	Af17-1-2a-2	2	C	910	0.5	0.5	SANDY_CLAY_LOAM
3	Af32-2ab-3	2	D	910	0.5	0.5	SANDY_CLAY_LOAM
4	Ao39-2b-4	2	C	1000	0.5	0.5	LOAM
5	Ao41-2bc-5	2	C	960	0.5	0.5	LOAM
6	Ao63-3b-6	2	C	1000	0.5	0.5	CLAY
7	Bc8-2b-7	2	C	820	0.5	0.5	LOAM
8	Bc9-2b-8	2	C	1000	0.5	0.5	CLAY_LOAM
9	Bd30-2-3c-9	2	C	560	0.5	0.5	CLAY_LOAM
11	Bd31-2c-11	2	B	370	0.5	0.5	LOAM
16	Be45-2a-16	2	C	980	0.5	0.5	LOAM
17	Be47-2a-17	2	C	1000	0.5	0.5	CLAY_LOAM
18	Be48-3c-18	2	C	440	0.5	0.5	CLAY
20	Be49-3c-20	2	C	760	0.5	0.5	CLAY
21	Be50-2-3c-21	2	C	820	0.5	0.5	CLAY_LOAM
22	Be51-2a-22	2	D	1000	0.5	0.5	CLAY_LOAM
24	Be8-3c-24	2	C	850	0.5	0.5	CLAY
26	Be9-3c-26	2	C	930	0.5	0.5	CLAY
27	Bh11-1b-27	2	B	1000	0.5	0.5	SANDY_LOAM

Environmental Implications of Cemetery Activities

The comprehensive study conducted on the second cemetery in Benin City, Edo State, Nigeria, reveals significant environmental implications associated with cemetery activities. The findings from geophysical surveys, soil analysis, and hydrological assessments provide insights into the pollution and potential risks to the surrounding environment.

1. Apparent Soil Pollution:

- ✓ Both dipole-dipole and vertical electric sounding (VES) studies indicate apparent soil pollution around the cemetery.
- ✓ Necroleachate, a contaminant resulting from the decomposition of bodies, is identified as a likely source of pollution.
- ✓ The topsoil in the vicinity of the cemetery is observed to be heavily contaminated, raising concerns for people, vegetation, and the built environment.

2. Elevation and Runoff:

- ✓ Elevation map (Figure 30) indicates that the cemetery is situated at a higher elevation than nearby residential areas.
- ✓ This elevation difference poses a risk as contaminants, including necroleachate, can be washed downhill into surrounding locations due to gravity.
- ✓ Soil erosion around cemeteries is noted as a contributing factor to the rapid spread of contaminants.

3. Soil Characteristics:

- ✓ Soil mapping (Figure 31) reveals a sandy-clay-loamy nature near the cemetery, validating the adequacy of VES results.
- ✓ The presence of clay in the third geoelectric layer, with a considerable thickness, confines contaminants to the topsoil.

4. Drainage Density and Runoff:

- ✓ Drainage density map (Figure 32) show the susceptibility of the cemetery to runoff, with higher drainage density indicating increased runoff potential.
- ✓ Limited vegetation around the cemetery contributes to higher runoff and the transportation of contaminants into neighboring areas.

5. Curve Number and Flooding Susceptibility:

- ✓ The curve number map (Figure 33) indicates a high curve number of 86.0 for the area around the cemetery, signifying high flooding susceptibility.

- ✓ Despite the thick layer of clay, gradual percolation of contaminants into the aquifer remains a concern, emphasizing the need for further investigation.

6. Groundwater Flow Direction:

- ✓ Groundwater flow direction map (Figure 34) reveals that necroleachate from the second cemetery is flowing in a north-easterly direction.
- ✓ Boreholes near Erhumwunse Street in the second cemetery are reported to be free from necroleachate, suggesting a localized impact.

Conclusion

The geophysical evaluation underscores the importance of understanding subsurface conditions for effective groundwater management. The evaluation of aquifer susceptibility near cemeteries in Benin City, Edo State, Nigeria, through geophysical techniques has provided valuable insights into the subsurface conditions and potential risks associated with groundwater contamination. The key findings from the vertical electric sounding (VES) and dipole-dipole study are summarized below:

- ✓ Both VES and dipole-dipole studies confirm the pollution of the topsoil near cemeteries in Benin City.
- ✓ The presence of contaminants, including necroleachate, is identified as a significant concern for the environment.
- ✓ The VES results reveal the existence of four distinct geoelectric layers in the subsurface near cemeteries. These layers include topsoil, lateritic soil, a weathered layer dominated by clay, and medium- to coarse-grained sand.
- ✓ The identification of subsurface layers and their resistivity, thicknesses, and depths contributes to a better understanding of the aquifer's vulnerability.
- ✓ The predominance of clay in the weathered layer acts as a barrier, preventing leachate from penetrating deeper into the subsurface.
- ✓ Clay serves a dual purpose as both a seal and a filter, limiting the downward movement of contaminants and mitigating groundwater contamination.

The study concludes that the thick layer of clay just below the topsoil effectively prevents leachate from entering the aquifer and the broader ecosystem thus enhancing the sustainability of groundwater resources in the vicinity of cemeteries.

Acknowledgements: *The authors are grateful to Tetfund (TETFUND/UNIBEN/N30/2020-2022 (MERGED) that provided the resources which the authors used in conducting the research.*

Funding: *This research was funded by Tetfund (TETFUND/UNIBEN/N30/2020-2022 (MERGED) through the project "Contaminant transport, statistical and geospatial analysis of groundwater quality around the vicinity of cemeteries in Benin City, Edo State Nigeria"*

Compliance with Ethical Standards Ethical responsibilities of Authors: *The author has read, understood, and complied as applicable with the statement on "Ethical responsibilities of Authors" as found in the Instructions for Authors".*

Conflict of Interest: *The authors declare that they do not have any conflict of interest.*

References

Adeyeye EI, Abulude FO, (2004) Analytical assessment to some surface and groundwater resources in Ile-Ife, *Nigeria. J. of Chem. Soc. Nigeria*. **29** (1) 98-103. https://www.scirp.org/reference/referencespapers?referenceid=2393410

Kudesia VP, Kudesia R, (2008) *Water Pollution*. KK. Mittal, Pragati Prakashan, Educational Publishers, Meerut, India. https://pragatiprakashan.in/products/water-pollution-839

Eugeniusz K, Andrzej T, Mariusz L, Piotr O, (2017) Application of Electrical Resistivity Data Sets for the Evaluation of the Pollution Concentration Level within Landfill Subsoil. *Appl. Sci. J.* **7** (262), 1-13. https://doi.org/10.3390/app7030262,

Asadi SS, Vuppala P, Reddy MA, (2007) Remote sensing and GIS techniques for evaluation of groundwater in Municipal Corporation of Hyderabad, India. *Int. J. Environ. Res. & Public Health*, **4** (1), 45-52. https://www.mdpi.com/1660-4601/4/1/45 https://doi.org/10.3390/ijerph2007010008

Debels P, Figueroa R, Urrutia R, Barra R, Niell X, (2005) Evaluation of water quality in the Chillan River (Central Chile) using physicochemical parameters and a modified water quality index.

Environmental Monitoring and Assessment, 110, 301–322. Retrieved from https://link.springer.com/article/10.1007/s10661-005-8066-5

Priyan K, (2021) Issues and challenges of groundwater and surface water management in semi-arid regions. In K Priyan (Ed.), *Groundwater Resources Development and Planning in the Semi-arid Region,* 1-17. https://www.amazon.com/Groundwater-Resources-Development-Planning-Semi-Arid/dp/3030681238

Sahoo S, Khaoash, S, (2020). Impact assessment of coal mining on groundwater chemistry and its quality from Brajrajnagar coal mining area using indexing models. *Journal of Geochemical Exploration, 215*, 106559. Retrieved from https://doi.org/10.1016/j.gexplo.2020.106559

Gleeson, T, Befus KM, Jasechko S, Luijendijk E, Cardenas MB, (2016) The global volume and distribution of modern groundwater. *Nature Geoscience, 9*, 161-167. Retrieved from https://www.nature.com/articles/ngeo2590

Üçisik AS, Rushbrook P, (1998) The Impact of Cemeteries on the Environment and Public Health; An Introductory Briefing. WHO Regional Office for Europe European Centre for Environment and Health Nancy Project Office. https://iris.who.int/bitstream/handle/10665/108132/EUR_ICP_EHNA_01_04_01(A).pdf

Żychowski J, (2012) Impact of cemeteries on groundwater chemistry; A review. *Catena, 9*, 29-37. https://zychowski.up.krakow.pl/download/CATENA1745_ostat.pdf

Bastianon, D, Matos, BA, Aquino, WF, Pacheco, A, Mendes, J, (2000). Geophysical surveying to investigate groundwater contamination by a cemetery; 13th EEGS Symposium on the Application of Geophysics to Engineering and Environmental Problems.

Lautz LK, Ledford SH, Beltran J, (2020) Legacy effects of cemeteries on groundwater quality and nitrate loads to a headwater stream. *Environmental Research Letters,* **15**, 1-11. Retrieved from https://iopscience.iop.org/article/10.1088/1748-9326/ab6a9f

Trick JK, Klinck BA, Coombs P, Chambers J, Noy DJ, West J, Williams GM, (2005) Groundwater impact of Danescourt cemetery, Wolverhampton Bringing Groundwater Quality Research to the Watershed Scale: Proc. of GQ 2004, the 4th Int. Groundwater Quality Conf. held at Waterloo (Canada July 2004) (IAHS Publ.), 297.

Trick JK, Klinck BA, Coombs P, Chambers J, Noy DJ, West J, Williams GM, (2001) Pollution potential of cemeteries: impact of Danescourt cemetery, Wolverhampton. British Geological Survey Internal Report, IR/01/104, 29, 1–26.

Abu-Bakr, HA, El-A, (2020) Groundwater vulnerability assessment in different types of aquifers. *Agric. Water Manag.,* **240**, 106275.

Bon AF, Sylvain AD, Lucian AB, Cyrille N, Steven C, Arouna MN, (2020) Contribution of a geostatistical model of electrical conductivity in the assessment of the water pollution index of the Quaternary aquifer of the Lake Chad basin (Kousseri-Cameroon). *Arab. J. Geosci.,* **13**, 170.

Ekanem AM, (2020) Geo-resistivity modelling and appraisal of soil water retention capacity in Akwa Ibom State University main campus and its environs, Southern Nigeria. *Model. Earth Syst. Environ.* Retrieved from https://doi.org/10.1007/s40808-020-00850-6.

Ekanem, AM, George, NJ, Thomas, JE, Nathaniel, EU, (2019). Empirical relations between aquifer Geohydraulic and Geoelectric properties derived from surficial resistivity measurements in parts of Akwa Ibom State, southern Nigeria. *Nat. Resour. Res., 09606-1*.

Aleke, CG, Ibuo, JC, Obiora DN, (2018). Application of electrical resistivity method in estimating geohydraulic properties of a sandy hydrolithofacies: a case study of Ajali Sandstone in Ninth Mile, Enugu State, Nigeria. *Arab J Geosci,* **11**, 322. Retrieved from Springer Link.

Dian Z, (2004). Land for the dead; locating urban cemeteries. A case study of Guilin, China. Thesis submitted to the International Institute for Geo-information Science and Earth Observation in partial fulfillment of the requirement for the degree of Ms. Sci. in Urban Planning and Administration, 1–86. Enschede, Netherlands.

Kabiru AT, Abubakar BSUI, Midaryu ND, Sangodoyin AY, (2019) Burial practice and its effect on groundwater pollution in Maiduguri, Nigeria. *Environ. Scie. & Pollut. Research*. Retrieved from Springer Link.

Egbai JC, Oseji JO, Ogala, JE, Emmanuel ED, (2019). Resistivity method applied to aquifer protection study in Agbor-obi and environs, Delta state, Nigeria. *Int J Appl Eng Res,* **14**(2), 373–383. Retrieved from Research India Publications.

Oseji, JO, Egbai, JC, (2019a). Aquifer characterization based on geoelectric survey data in Issele-Uku, Delta state, Nigeria. *Am Inst Phys Adv, 9*, 085124-1–085124-11.

Olla TA, Akinlalu AA, Olayanju GM, Adelusi AO, Adiat KAN, (2015) Geophysical and hydrochemical investigation of a municipal dumpsite in Ibadan, Southwest Nigeria. *J Environ Earth Sci,* **5**(14), 99–112. Retrieved from International Institute for Science, Technology and Education.

Ayuk M, Adelusi AO, Adiat KAN, (2013) Evaluation of groundwater potential and aquifer protective capacity assessment at Tutugbua-Olugboyega area, off Ondo-road, Akure Southwestern Nigeria. *Int J Phys Sci,* **8**(1), 37–50.

Awoniyi OO, (2013) Application of Geophysical Investigation to Evaluate the Impact of a Dumpsite on Groundwater: Case Study of Awotan-Apete, Ibadan. Unpublished M. Tech Thesis. Federal University of Technology, Akure.

Omosuyi GO, Oseghale A, (2012) Groundwater vulnerability assessment in shallow aquifers using geoelectric and hydrogeologic parameters at Odigbo, Southwestern Nigeria. *Am J Sci Ind Res,* **3**(6), 501–512. Retrieved from https://www.academicjournals.org/journal/AJSIR/article-full-text-pdf/81B5D9322535.

Thirumalaivasan D, Karmegam M, (2001) Aquifer Vulnerability Assessment using Analytical Hierarchy Process and GIS for Upper Palar Watershed. Center for Remote Imaging Sensing and Processing (CRISP). National University of Singapore.

Ehirim CN, Nwankwo CN, (2010) Evaluation of Aquifer Characteristics and Groundwater Quality Using Geoelectric Method in Choba, Port Harcourt. *Arch. Appl. Sci. Res.,* **2**, 396-403.

Foster, SSD (1998). Groundwater recharge and pollution vulnerability of British aquifers; a critical review. *Geol Soc London Special Publ,* **130**, 7-22.

Eluwole AB, Ademilua OL, (2014) Integrated Geophysical Investigations for the Development of a Sustainable Water Supply Scheme Within the Ekiti State University Campus, Ado-Ekiti, Southwestern, Nigeria. *Int J Sci Technol Res,* **3**(10), 294–304.

George NJ, (2020) Appraisal of hydraulic flow units and factors of the dynamics and contamination of hydrogeological units in the littoral zones: a case study of Akwa Ibom State University and its Environs, Mkpat Enin LGA, Nigeria. *Nat Resour Res*. Retrieved from Springer Link.

George NJ, (2021) Modelling the trends of resistivity gradient in hydrogeological units: a case study of alluvial environment. *Model Earth Syst Environ,* **7**, 95–104. Retrieved from https://doi.org/10.1007/s40808-020-01021-3.

Anomohanran O, (2011) Underground water exploration of Oleh, Nigeria using the electrical resistivity method. *Sci Res Essays, 6(20)*, 4295–4300. https://www.academicjournals.org/journal/SRE/article-full-text-pdf/081162219647

Ayolabi, EA, Atakpo, EA, Otobor, EC, Arerin, T, (2009). Groundwater quality assessment using predrilling electrical measurement. *J Environ Hydrol,* **17**, 10–15. https://www.interstatepublishers.com/journal/JEH/article-full-text-pdf/6D1162270933

Oseji, JO, Egbai, JC, Okolie, EC, Ese, EC, (2018). Investigation of the aquifer protective capacity and groundwater quality around some open dumpsites in Sapele Delta state, Nigeria. *Appl Environ Soil Sci*. http://www.ripublication.com/ijaer18/ijaerv13n4_38.pdf

Oseji JO, Egbai JC, (2019b) Geoelectric assessment of groundwater prospects and vulnerability of overburdened aquifer in Oleh, Delta state, Nigeria. *Int J Appl Eng Res, 14(3)*, 806–820. http://www.ripublication.com/ijaer19/ijaerv14n3_27.pdf

Cristina P, Cristina D, Alicia F, Pamela B, (2012) Application of Geophysical Methods to Waste Disposal Studies. In X-Y Yu (Ed.), *Municipal and Industrial Waste Disposal, 1-5*. Intech Open. https://doi.org/10.5772/29615

Abdullahi, NK, Osazuwa, IB, Sule, PO, (2011). Application of Integrated Geophysical Techniques in the Investigation of Groundwater Contamination. A Case Study of Municipal Solid Waste Leachate. *Ozean J Appl Sci,* **4**, 7-25.

Jegede SI, Ujuanbi, O Abdullahi NK, Iserhien-Ewekeme, RE, (2012) Mapping and Monitoring of Leachate Plume Migration at an Open Waste Disposal Site Using Non-Invasive Methods. *Res J Environ Earth Sci,* **4**, 26-33. https://www.academicjournals.org/article/article1621384312_Jegede%20et%20al.pdf

Ganiyu SA, Badmus BS, Oladunjoye MA, Aizebeokhai AP, Olurin OT, (2015) Delineation of Leachate Plume Migration Using Electrical Resistivity Imaging on Lapite Dumpsite in Ibadan, Southwestern Nigeria. *Geosciences,* **5***,* 70-80. https://www.mdpi.com/xxx

Giang NV, Kochanek K, Vu NT, Duan NB, (2018). Landfill Leachate Assessment by Hydrological and Geophysical Data: Case Study NamSon, Hanoi, Vietnam. *J Mater Cycles Waste Manage, 20*, 1648-1662. https://doi.org/10.1007/s10163-018-0732-7

Ayolabi, EA, Adetayo, FF, Olusola, TK, (2013). Integrated Geophysical and Geochemical Methods for Environmental assessment of Municipal Dumpsite System. *Int J Geosci, 4*, 850-862. https://doi.org/10.4236/ijg.2013.45079

Ikhile CI, (2016) Geomorphology and Hydrology of the Benin Region, Edo State, Nigeria. *Int J Geosci,* **7**(2)*,* 144-157. https://doi.org/10.4236/ijg.2016.72012

Idehai IM, Egai AO, (2014) Aspects of Geophysical Exploration for Groundwater Using Vertical Electrical Sounding (VES) in Parts of University of Benin, Benin City, Edo State. *J Appl Sci Environ Manage,* **18**(1)*,* 19-25. http://www.ripublication.com

Orakwe LO, Olorunfemi MO, Ofoezie IE, Oni AG, (2018) Integrated Geotechnical and Hydrogeophysical Investigation of the Epe Wetland Dumpsite in Lagos State, Nigeria. *Ife J Sci,* **20**(3)*,* 461-473.

Ugwuanyi MC, Ibuot JC, Obiora DN, (2015) Hydrogeophysical study of aquifer characteristics in some parts of Nsukka and Igbo Eze South local government areas of Enugu State, Nigeria. *Int J Phys Sci, 10(15)*, 425-435. http://www.academicjournals.org/IJPS

Obiora DN, Ibuot JC, George NJ, (2016). Evaluation of aquifer potential, geoelectric and hydraulic parameters in Ezza North, southeastern Nigeria, using geoelectric sounding. *Int J Environ Sci Technol, 13*, 435-444. https://doi.org/10.1007/s13762-016-0991-2

Lashkaripour GR, Nakhaei M, (2005) Geoelectrical investigation for the assessment of groundwater conditions: a case study. *Ann Geophys,* **48**(6)*,* 937-944. https://www.annalsofgeophysics.eu/index.php/ annals/article/view/3428

Gemail KS, El-Shishtawy, AM, El-Alfy, M, Ghoneim, MF, Abd-elbary MH, (2011) Assessment of aquifer vulnerability to industrial wastewater using resistivity measurements: a case study along El-Gharbyia main Drain, Nile Delta, Egypt. *J Appl Geophys,* **75**, 140-150. https://doi.org/10.1016/j.jappgeo.2011.08.002

Kearey P, Brooks M, Hill I, (2002) An Introduction to Geophysical Exploration, 3rd Ed. Blackwell Publishing, pp. 183-207.

Hubbard S, Rubin Y, (2006) Hydrogeological characterization using geophysical methods. In *The Handbook of Groundwater Engineering*, edited by Delleur, J. CRC Press, New York, Chap. 14, pp. 1-52.

Iserhien-Emekeme RE, Atakpo EA, Emekeme OL, Anomohanran O, (2004) Geoelectric survey for groundwater in Agbede, Etsako West LGA, Edo State. *Adv Nat Appl Sci Res, 2*, 65-72.

Spongberg AL, Becks PM, (2000) Inorganic soil contamination from cemetery leachate. *Water Air Soil Pollut,* **117**, 313-327.

Jonker C, Olivier J, (2012) Mineral Contamination from Cemetery Soils: Case Study of Zandfontein.

Schenk, ER, O'Donnell, F, Springer, AE, Stevens, LE, (2020). The impacts of tree stand thinning on groundwater recharge in arid land forests. *Ecol Eng, 145*, 105701. https://doi.org/10.1016/J.ecoleng.2019.105701

Simsek C, Kincal C, Gunduz O, (2006) A solid waste disposal site selection procedure based on groundwater vulnerability mapping. *Environ Geol, 24*, 620-633.

Sen PN, Goode PA, Sibbit A, (1988) Electrical conduction in clay bearing sandstones at low and high salinities. *J Appl Phys, 63*, 4832-4840.

Rottger B, Kirsch R, Scheer W, Thomsen S, Friborg R, Voss W, (2005) Multifrequency airborne EM surveys - a tool for aquifer vulnerability mapping. In: Butler, DK (ed) *Near Surface Geophysics*, Investigations in Geophysics, Society of Exploration Geophysicists, Tulsa, 13, 643-651.

Casas A, Himi M, Diaz Y, Pinto V, Font X, Tapias JC, (2008) Assessing aquifer vulnerability to pollutants by electrical resistivity tomography (ERT) at a nitrate vulnerable zone in NE Spain. *Environ Geol, 54*, 515-520. https://ui.adsabs.harvard.edu/abs/2008EnGeo..54..515C/abstract

Hirabayashi Y, Mahendran R, Koirala S, Konoshima L, Yamazaki D, Watanabe S, Kim H, Kanae S, (2013). Global flood risk under climate change. *Nat Clim Change, 3*, 816. https://www.nature.com/articles/nclimate1911

Sofia G, Roder G, Dalla Fontana G, Tarolli P, (2017) Flood dynamics in urbanized landscapes: 100 years of climate and human's interaction. *Sci Rep, 7*, 40527. https://www.nature.com/articles/srep40527.pdf

J. Int. Environmental Application & Science, Vol. **19**(3): 151-159 (2024)
Research Paper

Adsorption of Anionic Dyes Using Turkish Coffee Waste: Efficiency and Mechanism

Özgül Çimen Mesutoğlu*

Department of Environmental Engineering, Aksaray University, Aksaray, Turkey

Received September 2;2024; Accepted September 30, 2024

Abstract: Turkish coffee waste (TCW), an organic by-product, was employed for the adsorption-based removal of Reactive Red 195 (RR195) dye from aqueous solutions. The study explored various parameters including pH (ranging from 3 to 9), initial RR195 concentration (5-500 mg/L), contact time (1-360 minutes), and amount of adsorbent (0.5-20 g/L). In a batch system, these experiments achieved a significant removal efficiency of 89% under optimal conditions. The pseudo-second order (PSO) kinetic model provided the most accurate representation of the kinetics of RR195 removal by TCW. Additionally, the adsorption equilibrium data aligned well with the Freundlich isotherm model. The maximum adsorption capacity of TCW for RR195 was found to be 63.5 mg/g under these optimum conditions; pH=7, RR195=500 mg/L, contact time=60 min., amount of TCW=7 g/L. These findings confirm that TCW can effectively remove RR195 through adsorption without requiring any pre-treatment.
Keywords: *Adsorption, Low-Cost adsorbent, Reactive red 195, Turkish coffee waste*

Introduction

Reactive Red 195 (RR195) is a widely used azo dye in the textile industry, known for its vibrant red colour. This dye is preferred for its strong binding affinity to cellulosic fibers, which enhances wash fastness and ensures long-lasting coloration (Katheresan *et al.,* 2018). However, the extensive use of RR195 leads to significant environmental concerns, as large quantities of untreated dye are discharged into wastewater. The dye's complex molecular structure, particularly the sulfonic acid groups that facilitate its solubility in water, makes its removal from wastewater challenging using conventional treatment methods (Saratale *et al*., 2019). Consequently, there is increasing interest in developing more efficient and sustainable techniques for the removal of RR195 from industrial effluents, including advanced oxidation processes, biological treatment methods, and the use of novel adsorbents. These efforts are crucial for reducing the environmental impact of textile dyeing processes and promoting more sustainable practices within the industry (Verma *et al*., 2021).

Various methods can be employed for the treatment of RR195. Chemical oxidation techniques effectively remove these dyes from aqueous environments (Sirés & Brillas, 2012; Deng & Zhao, 2015). Processes involving oxidants such as ozonation, hypochlorite, and peroxide aid in breaking down the dye and preventing the formation of harmful byproducts. Among physical methods, adsorption using activated carbon or other adsorbent materials is commonly used to remove the dye from water (Rafatullah *et al*., 2010; Bhatnagar *et al*., 2013). Additionally, biological treatment methods can be applied, wherein specific bacteria or enzymes are utilized to biologically degrade the dye (Ahuja *et al*., 2018). Advanced treatment techniques typically involve a combination of these methods, thereby enhancing the efficiency of the treatment process. The selection of these various treatment methods depends on the characteristics of the dye used and the capacity of the treatment facility (Zhang *et al*., 2014; Kumar *et al*., 2019). Due to the substantial global consumption of coffee, estimated at approximately 8 million metric tons annually, coffee waste is a widely available biowaste that holds significant potential as a precursor for adsorbent synthesis (Zuorro & Lavecchia, 2020).

This study examines the use of TCW, a natural waste material, as an adsorbent for the adsorption of RR195. The research evaluates the effects of key adsorption parameters, such as pH, contact time, amount of adsorbent, and initial concentration, on the adsorption efficiency of RR195 onto TCW. Additionally, the adsorption kinetics and mechanisms are systematically analyzed and calculated to provide a deeper understanding of the adsorption process.

*Corresponding: E-Mail: ozgulcimen@gmail.com, Tel: (+90382)288 36 06. Fax: (090382)288 35 25

Material and Method

Adsorbent and Dye Preparation

In Turkey, Turkish coffee is highly popular and widely consumed by people. Turkish coffee is made by grinding coffee beans to a particle size of approximately 200 µM. Due to the high daily consumption of this coffee, significant amounts of coffee waste are generated. This raises the potential for its use as a low-cost natural adsorbent.

Before being used as an adsorbent, TCW was subjected to an extensive cleansing procedure, which involved repeated rinsing with distilled water to remove any surface impurities. The process, though necessary, seemed endless, as if the contaminants were always just out of reach, clinging stubbornly to the surface. After that, dried at 60°C for 24 hours. Thus, adsorbent was prepared. RR195 dye (Sigma-Aldrich) in powder form were used to produce stock solutions (1000 mg/L), which were then diluted to produce dyes solutions with desired concentrations. The chemical structures of the RR195 dye, TCW and RR195 adsorption images are illustrated in Figure 1.

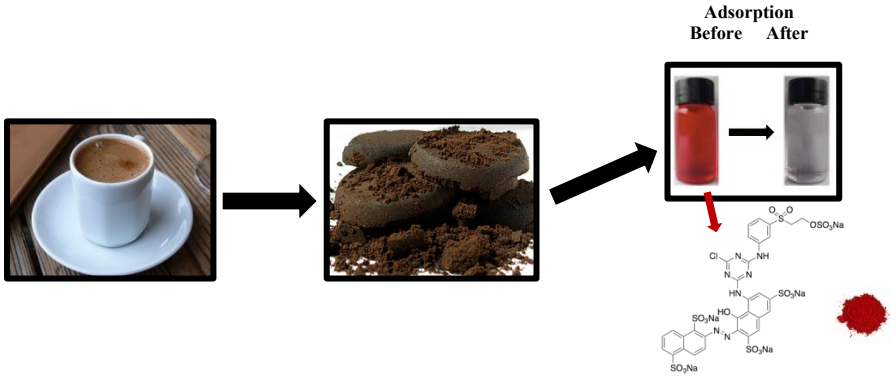

Figure 1. RR195 chemical structure, TCW and RR195 adsorption images.

Isotherm and Kinetic Study

The Langmuir adsorption isotherm (Langmuir, 1918) describes the monolayer adsorption of a solute onto a surface with a limited number of identical binding sites. The model operates on several key assumptions: (i) adsorption occurs in specific, homogeneous regions of the adsorbent; (ii) each dye molecule occupies a single site; (iii) the adsorbent has a fixed capacity for the pollutant at equilibrium; and (iv) all adsorption sites are uniform and possess equal energetic properties. In contrast, the Freundlich isotherm model (Freundlich, 1906) accounts for the heterogeneity of the adsorptive surface, allowing for multilayer adsorption and variation in site energy distribution. The Temkin isotherm model (El-Shafie, 2023) proposes that the heat of adsorption decreases linearly as more molecules are adsorbed, indicating uniform binding energy across the surface. Meanwhile, the Dubinin-Radushkevich (D-R) isotherm (Laskar & Hashisho, 2020) is grounded in potential theory and is particularly applicable to adsorption on heterogeneous surfaces. Kinetic models are used to explore the mechanisms underlying pollutant adsorption onto the adsorbent surface. This study aims to provide insights into these mechanisms and pollutant-adsorbent interactions, enabling the formulation of appropriate mathematical models for their characterization. The pseudo-first order (PFO) and pseudo-second order (PSO) have been applied to describe the adsorption process (Lagergren, 1898; Ho & McKay, 1999; Ho *et al*., 2000). A summary of the isotherm and kinetic equations, along with their relevant parameters, is provided in Table 1.

Table 1. Isotherms and kinetic parameters related to adsorption of RR195

Model	Equation	Parameter	References
Isotherm Model			
Langmuir	$\frac{C_e}{q_e} = \frac{C_e}{q_m} + \frac{1}{K_L q_m}$ $R_L = \frac{1}{1 + K_L C_0}$	q_m (mg/g): Maximum adsorption capacity C_e (mg/L): Adsorbate concentration at equilibrium q_e (mg/g): Amount of adsorbate uptake at equilibrium	Langmuir, 1918

Freundlich	$\ln q_e = \ln K_F + \frac{1}{n}\log C_e$	K_L (L/mg): Langmuir coefficients R_L: Langmuir separation factor K_F (mg/g) (L/mg)^n and n: Freundlich coefficients R (8.314 J/molK): Gas constant	Freundlich, 1906
Temkin	$q_e = \frac{RT}{b_T}\ln A_T + \frac{RT}{b_T}\ln C_e$	A (L/g): Temkin isotherm constant T (K): Adsorption temperature	Inyinbor, 2016
D-R	$B = {}^{RT}/_{b_T}$ $lnq_e = lnq_m - k_{ad}\varepsilon^2$ $\varepsilon = RT\ln\left(1+\frac{1}{C_e}\right)$ $E = (2\ x\ K_{ad})^{-1/2}$	q_s (mg/g): Adsorption capacity K_{ad} (mol^2/kj): Dubinin–Radushkevich isotherm constant ε: Dubinin–Radushkevich isotherm constant E (kJ/mol): Mean adsorption energy	Güneş, 2023
Kinetic Model			
PFO	$\ln(q_e - q_t) = \ln q_e - k_1 t$	q_t (mg/g): Adsorption capacity at time t t (min): Time k_1 (1/min): The pseudo first-order model rate constant	Lagergren, 1898
PSO	$\frac{t}{q_t} = \frac{1}{k_2 q_e^2} + \frac{1}{q_e}t$	k_2 (g/mg.min): The pseudo second-order rate constant	Ho & McKay, 1999

Adsorption studies

Adsorption experiments were carried out using a thermostatic shaker (Nüve SL350) with a solution volume of 1 L and a constant shaking rate of 200 rpm. After testing various agitation speeds, it was determined that the optimal speed is 200 rpm. To examine the impact of contact time on the removal efficiency of RR195, tests were performed at different time intervals, spanning from 2 minutes to 360 minutes. The influence of amount of adsorbent on RR195 removal was assessed using different amounts of TCW, varying from 0.5 to 20 g/L. The effect of pH on RR195 adsorption was evaluated by performing experiments within a pH range of 3 to 9. Additionally, the impact of initial dye concentration on removal efficiency was examined using seven different concentrations, ranging from 5 to 500 mg/L. For the analysis of the effects of amount of adsorbent, pH, contact time, temperature, and initial dye concentration, samples were centrifuged at 3000 rpm for 4 minutes using a Nüve CN180 centrifuge. The resulting supernatants were then analyzed using a UV-Vis spectrophotometer. The residual dye concentration in the solution after adsorption was determined at 542 nm. From the experimental data, equilibrium concentration (C_e), adsorption capacity (q_e), and percentage removal rates were calculated according to Eq. (1) and Eq. (2).

$$RR195\ removal\ (\%) = \frac{C_0 - C_e}{C_0} x100 \quad (1)$$

$$q_e = \frac{(C_0 - C_e).V}{m} \quad (2)$$

C_o is initial concentration of RR195, C_e (mg/L) is final concentration of RR195. m (g) represents the mass of TCW. The volume of the solution is presented with V (L), where q_e (mg/g) is the amount of adsorbed RR195 by TCW.

Determination of the Point of Zero Charge (pH_{pzc}) for TCW

For this study, the methodology outlined by Aguilar *et al*. (2020) was applied to determine the pH_{pzc} of the adsorbent selected for the removal of RR195 from TCW. Based on this approach, the adsorption mechanism was analyzed, providing insights into the processes potentially involved during adsorption.

Characterization of TCW

The FTIR spectra corresponding to TCW are presented in Figure 2. TCW exhibits peaks that correspond to numerous functional groups.

FTIR analysis of TCW provides essential insights into the chemical structure of the organic components present in the material. The typical FTIR spectrum of TCW reveals several characteristic bands that correspond to different functional groups. The broad band observed in the range of 3300-3500 cm^{-1} is associated with O-H stretching vibrations (Dolatabadi *et al*., 2018), indicative of hydroxyl groups, which are prevalent in water, cellulose, and phenolic compounds found in coffee waste. The bands appearing between 2850-2950 cm^{-1} correspond to C-H stretching vibrations of aliphatic hydrocarbons, suggesting the presence of lipids and other aliphatic components. The distinct band observed around 1700-1735 cm^{-1} is attributed to C=O stretching vibrations (Litefti *et al.,* 2019), highlighting the presence of carbonyl groups from esters, acids, or ketones. Additionally, the band in the 1600-1650 cm^{-1} range indicates C=C stretching vibrations, pointing to the presence of aromatic rings, likely from lignin or other phenolic compounds (Igwegbe *et al.,* 2019). The 1400-1450 cm^{-1} region corresponds to C-H bending vibrations, while the 1000-1200 cm^{-1} region is associated with C-O stretching vibrations, representing the presence of alcohols, esters, and ethers. Finally, bands in the 900-750 cm^{-1} range indicate aromatic ring bending vibrations, further confirming the presence of lignin (Zahir *et al*., 2024). These spectral features highlight the complex organic composition of TCW, making it a valuable resource for applications in biofuel production, biomaterial development, and other sustainable technologies.

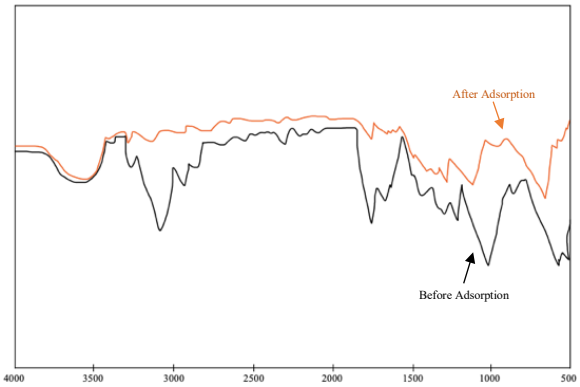

Figure 2. FTIR spectra of TCW

Results and Discussions

Effect of operating parameters on RR195 removal

The pH_{pzc} is a critical parameter in adsorption studies, as it defines the pH at which the adsorbent surface carries a neutral charge. At pH values below the pH_{pzc}, the adsorbent surface becomes positively charged, enhancing the adsorption of negatively charged species through electrostatic attraction (Yan *et al*., 2018). Conversely, at pH values above the pH_{pzc}, the surface acquires a negative charge, promoting the adsorption of positively charged molecules. Determining the pH_{pzc} is essential for optimizing adsorption processes, as it allows for the prediction of adsorption behaviour under different pH conditions. For instance, in the adsorption of dyes or heavy metals, knowing the pH_{pzc} can help in selecting the most favourable pH environment to maximize removal efficiency (Zhu *et al*., 2020). This parameter is particularly significant when dealing with heterogeneous adsorbents, where surface charge variation plays a vital role in the overall adsorption mechanism.

Figure 3 illustrates a non-linear relationship between the initial and final pH values. The high pH_{pzc} (8) of TCW indicates an abundance of positive charges on the adsorbent surface, which can only be fully neutralized under alkaline conditions.

In this adsorption study, key parameters such as pH, amount of adsorbent, initial RR195 concentration, and contact time were carefully evaluated. Comprehensive results for each of these factors are presented in Figure 4. The adsorption performance of the systems was found to be strongly influenced by pH, as it alters the ionization state of functional groups on both the adsorbate and the adsorbent. Thus, identifying the optimal pH for RR195 adsorption onto TCW is essential. To determine

this, experiments were conducted over a pH range of 3 to 9, with varying initial dye concentrations, solid-to-liquid ratios between 0.5 and 20 g/L, and at a constant temperature of 25°C. The amount of adsorbent is a crucial factor in defining the removal capacity in the adsorption process. Therefore, the amount of TCW was systematically varied from 0.5 to 20 g/L, while keeping pH and temperature constant at 25°C. The removal efficiency of TCW improved significantly, reaching up to 87%. As the amount of adsorbent increased, the removal efficiency of RR195 also increased, which can be attributed to the greater availability of active binding sites. Initially, the removal efficiency increased as the amount of adsorbent was raised from 0.5 g to 20 g/L, reaching up to 7 g/L, after which it stabilized. However, the adsorption capacity declined, likely because at lower adsorbent doses, more active sites remain accessible on the surface. In the study, the RR195 removal rate was rapid during the initial minutes of contact, with equilibrium being reached after approximately 60 minutes. The high removal efficiency observed during the early stages of adsorption is likely due to the increased active surface area of the adsorbent. For initial RR195 concentrations ranging from 5 to 500 mg/L, a removal efficiency of 89% was achieved within the first 60 minutes. Based on the overall analysis, the optimal conditions for RR195 adsorption using TCW were determined as follows: a contact time of 60 minutes, 7 g/L amount of TCW, an initial RR195 concentration of 500 mg/L, and a pH of 7. The adsorption process was further conducted at a temperature of 25°C, using a solution volume of 1 L and an agitation speed of 200 rpm.

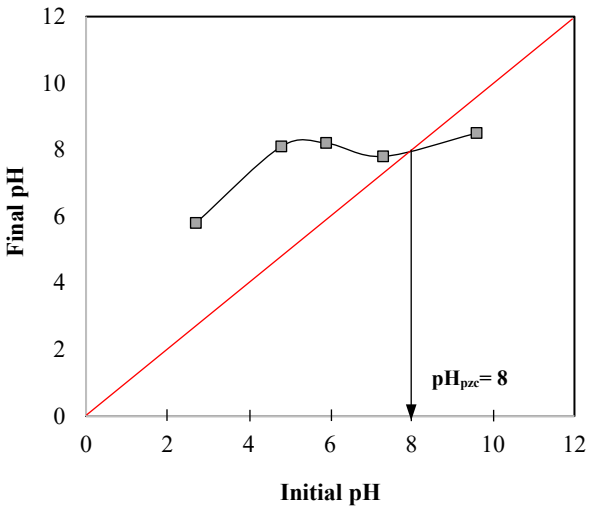

Figure 3. Determination of pH_{pzc} for TCW

Kinetic and Isotherm Study

Equilibrium data, commonly known as adsorption isotherms, are crucial for the characterization and design of adsorption systems. These data provide a mathematical relationship between the amount of adsorbate per unit of adsorbent at equilibrium and the concentration remaining in the solution. Isotherm studies were performed by treating RR195 dye solutions with initial concentrations varying from 5 to 500 mg/L, at a constant temperature of 25°C, for a fixed contact time of 60 minutes. Figure 5 provides the constants of Langmuir, Freundlich, Temkin, and D-R isotherm models. Freundlich model is a better fit for the adsorption data of RR195, as indicated by the higher R^2 values than other models. According to these results, the Freundlich adsorption isotherm model indicates that the adsorption process is multi-layered. And that adsorption occurs on a heterogeneous surface, and each layer is homogeneous and monolayered, as described in the Langmuir model. Additionally, since the adsorption mechanism occurs based on weak van der Waals forces, it can be considered a physical process.

The correlation coefficient for the PSO kinetic model is found to be high (0.98) (Figure 6). The calculated equilibrium adsorption capacity of TCW is 61.9 mg/g, which is consistent with the experimental value of 63.5 mg/g. The strong correlation provided by the PSO kinetic model suggests that the adsorption of RR195 onto TCW follows a multi-step process, involving both surface sorption and diffusion into the adsorbent. Furthermore, the excellent fit of the PSO kinetic model indicates that chemical sorption, involving valence forces through electron exchange or sharing between the TCW adsorbent and RR195 dye molecules, could be the rate-controlling step and play a significant role.

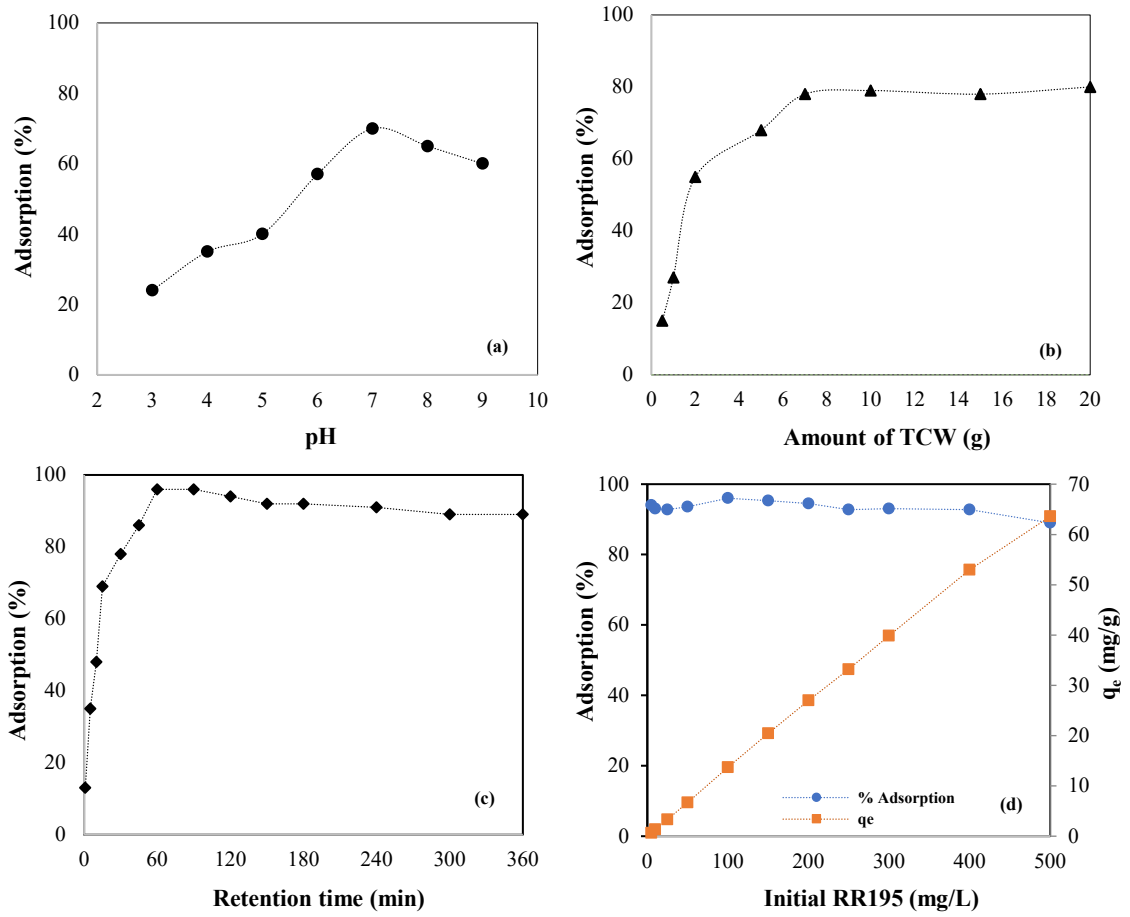

Figure 4. Effects of **(a)** solution pH, **(b)** amount of TCW, **(c)** retention time, and **(d)** initial RR195 concentration on adsorption process

The literature includes various studies involving different adsorbents and dyes. Some of these studies are summarized in Tab. 2. When comparing adsorption capacities, the type of adsorbent material and the dye used are significant factors**.**

Table 2. Evaluation of RR195 adsorption studies with various adsorbents

Adsorbent	**Dye**	**q_e (mg/g)**	**References**
Coffee waste	Congo Red	34.36	Wong *et al.,* 2020
	Reactive Black 5	77.52	
Banana peel powder	Reactive Black 5	49.2	Munagapati *et al.,* 2018
Soybean leaves	RR195	12	Mahanna & Samy, 2020
Coffee husk	RR195	188.12	Thi *et al.,* 2021
Lotus leaf powder	RR195	131.5	Munagapati *et al.,* 2021
Sunflower husks	RR195	9.5	Alhares *et al.,* 2023
	RB49	9.3	
TCW	RR195	63.5	This study

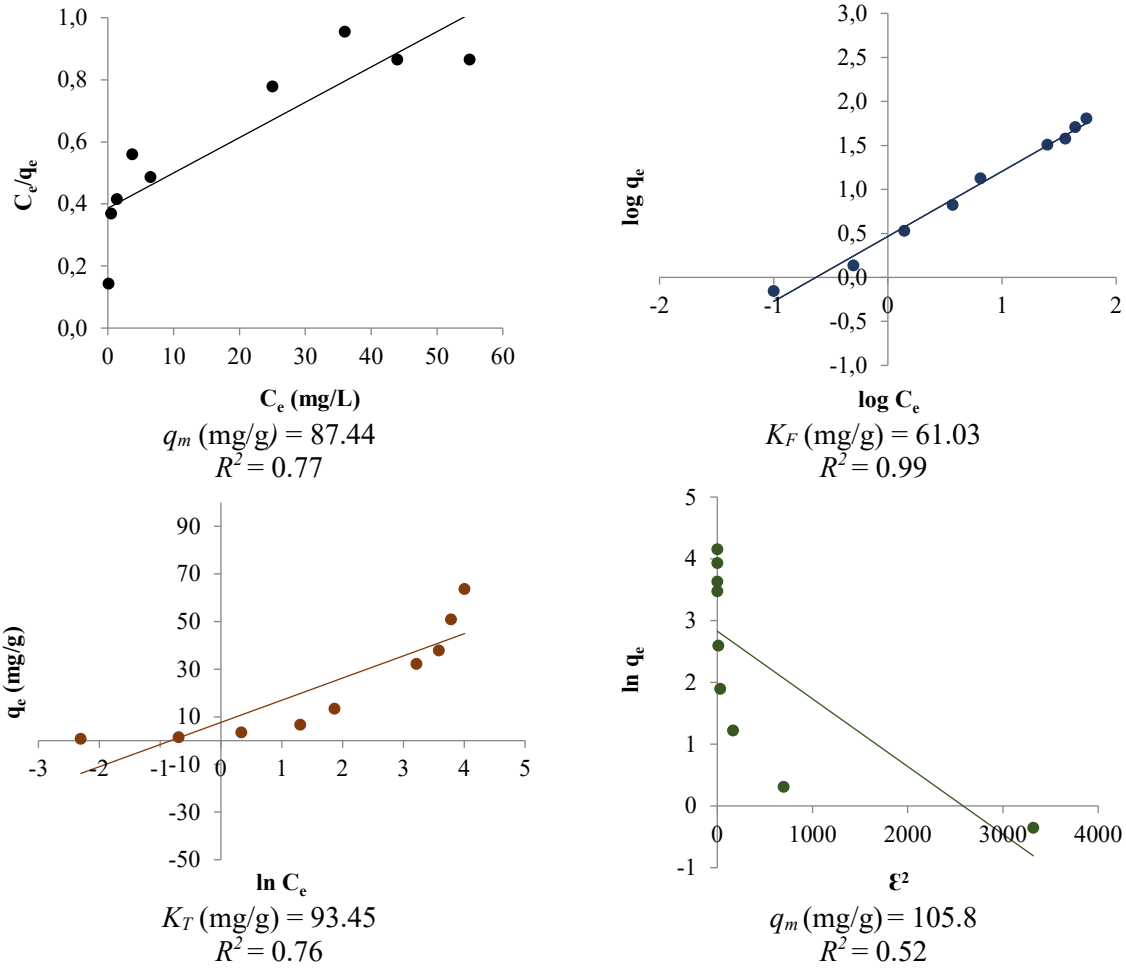

Figure 5. Langmuir, Freundlich, Temkin and D-R isotherm results

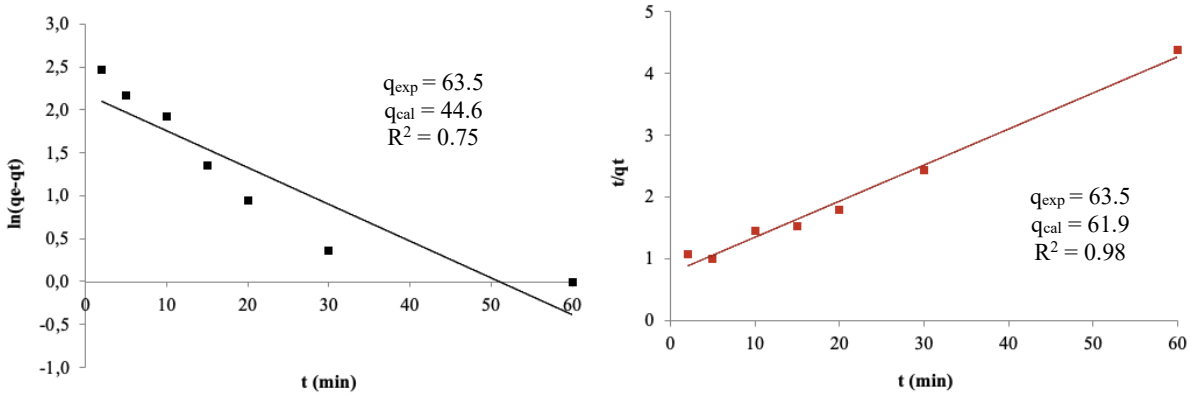

Figure 6. PFO and PSO kinetic results

Conclusion

This study investigated the removal of RR195 dye using TCW through an adsorption method in a laboratory setting. The adsorption process was examined with respect to various parameters including pH (3-9), initial concentration of RR195 (5-500 mg/L), amount of TCW (0.5-20 g), and contact time (2-360 minutes). Optimal conditions for maximum removal efficiency were found to be pH 7, TCW amount of 7 g, initial RR195 concentration of 500 mg/L, and contact time of 60 minutes. The maximum adsorption capacity of TCW was calculated to be q_e=63.5 mg/g. According to the results from the isotherm study, the Freundlich isotherm model best describes the adsorption mechanism among the applied isotherm equations. Additionally, the adsorption kinetics were best represented by the pseudo-second-order kinetic model. It was determined that TCW is suitable for the adsorption of RR195.

Additionally, the fact that TCW was used without any thermal or chemical pre-treatment is a significant aspect of the study.

Declarations: *Author has read, understood, and has complied as applicable with the statement on "Ethical responsibilities of Authors" as found in the Instructions for Authors.*
Availability of data and material: *Not applicable.*
Competing interests: *The author declares no financial and non-financial competing interests.*
Funding: *No funding was obtained for this study.*
Authors' contributions: *The article was written entirely by Özgül Çimen Mesutoğlu.*

References

Alhares HS, Shaban MAA, Salman MS, M-Ridha MJ, Mohammed SJ, Abed KM, Inrahim MA, Al-Banaa AK, Hasan HA, (2023) Sunflower Husks Coated with Copper Oxide Nanoparticles for Reactive Blue 49 and Reactive Red 195 Removals: Adsorption Mechanisms, Thermodynamic, Kinetic, and Isotherm Studies. *Water Air Soil Poll.,* **234**, 35. https://doi.org/10.1007/s11270-022-06033-6

Ahuja S., et al. (2018) Biosorption of Reactive Red 195 using Saccharomyces cerevisiae: Optimization and kinetic studies. *Journal of Environmental Chemical Engineering*, **6**(3), 3561-3568.

Aguilar DLG, Rodríguez Miranda JP, Miller MXA, Astudillo RIM, Muñoz JAE, (2020) Removal of Zn(II) in synthetic wastewater using agricultural wastes. *Metals*, **10**, 1465. https://doi.org/10.3390/met10111465

Bhatnagar A, Hogland W, Marques M, Sillanpää M, (2013) An overview of the modification methods of activated carbon for its water treatment applications. *Chem. Engin. J.*, **219**, 499-511. https://doi.org/10.1016/j.cej.2012.12.038

Dolatabadi M, Mehrabpour M, Esfandyari M, Alidadi H, Davoudi M, (2018) Modeling of simultaneous adsorp- tion of dye and metal ion by sawdust from aqueous solution using of ANN and ANFIS. *Chemometrics and Intelligent Laboratory Systems*, **181**, 72–78. https://doi.org/10.1016/j.chemolab.2018.07.012

El-Shafie M, (2023) A comprehensive assessment of ammonia synthesis reaction kinetics and rate equations. *Int. J. Hyd. Energy*, **48**, 35938-35952. https://doi.org/10.1016/j.ijhydene.2023.06.011

Freundlich HM, (1906) Over the Adsorption in Solution. *J. Physical Chem. A,* **57**, 385-470.

Güneş K, (2023) Isotherm and kinetic modeling of the adsorption of methylene blue, a cationic dye, on pumice. *Int. J. Chem. & Tech.*, **7**(1), 67- 74.

Ho YS, McKay G, (1999) Pseudo-second order model for sorption processes, *Process Biochemistry*, **34**, 451–465. https://doi.org/10.1016/S0032-9592(98)00112-5

Ho JHN, Kallstrom G, Johnson AW, (2000) Nmd3p is a Crm1p-dependent adapter protein for nuclear export of the large ribosomal subunit. *J. Cell Bio.,* **151**(5), 1057-1066. https://doi.org/10.1083/jcb.151.5.1057

Igwegbe CA, Mohmmadi L, Ahmadi S, Rahdar A, Khadkhodaiy D, Dehghani R, Rahdar S, (2019). Modeling of adsorption of methylene blue dye on Ho-$CaWO_4$ nanoparticles using response surface methodology (RSM) and artificial neural network (ANN) techniques. *MethodsX*, **6,** 1779–1797.

Inyinbor AA, Adekola FA, Olatunji GA, (2016) Kinetics, isotherms and thermodynamic modeling of liquid phase adsorption of Rhodamine B dye onto Raphia hookerie fruit epicarp, *Water Resources & Industry,* **15**, 14-27. https://doi.org/10.1016/j.wri.2016.06.001.

Katheresan V, Kansedo J, Lau SY, (2018) Efficiency of various recent wastewater dye removal methods: A review. *J. Environ. Chem. Engin.*, **6**(4), 4676-4697. https://doi.org/10.1016/j.jece.2018.06.060

Kumar, A., et al. (2019) Integration of advanced oxidation processes with biological treatments: An emerging strategy for wastewater treatment. *Science of the Total Environment*, 696, 133989.

Lagergren S, (1898) About the theory of so-called adsorption of soluble substances. *Kungliga Svenska Vetenskapsakademiens Handlingar,* **24**, 1-39.

Langmuir I, (1918) The Adsorptıon of Gases on Plane Surfaces of Glass, Mica and Platinum. *J. Am. Chem. Soc.,* **40**(9), 1361–1403.

Laskar II, Hashisho Z, (2020) Insights into modeling adsorption equilibria of single and multicomponent systems of organic and water vapors. *Separ. & Purif. Tech.,* **241**, 116681. https://doi.org/10.1016/j.seppur.2020.116681

Litefti K, Freire MS, Stitou M, González-Álvarez J, (2019) Adsorption of an anionic dye (Congo red) from aqueous solutions by pine bark. *Sci.Reports,* **9**, 16530. https://doi.org/10.1038/s41598-019-53046-z

Mahanna H, Samy M, (2020) Adsorption of Reactive Red 195 dye from industrial wastewater by dried soybean leaves modified with acetic acid, *Desal. & Water Treat.* **178**, 312–321.

Munagapati VS, Yarramuthi V, Kim Y, Lee KM, Kim DS, (2018) Removal of anionic dyes (reactive black 5 and congo red) from aqueous solutions using banana peel powder as an adsorbent. *Ecotox. & Environ. Safety*, **148**, 601–607.

Munagapati VS, Wen HY, Wen JC, Gollakota ARK, Shu CM, Lin KYA, Wen JH, (2021). Adsorption of Reactive Red 195 from aqueous medium using Lotus (Nelumbo nucifera) leaf powder chemically modified with dimethylamine: characterization, isotherms, kinetics, thermodynamics, and mechanism assessment. *Int. J. Phytorem.,* **24**(2), 131–144. https://doi.org/10.1080/15226514.2021.1929060

Rafatullah M, Sulaiman O, Hashim R, Ahmad A, (2010) Adsorption of methylene blue on low-cost adsorbents: A review. *J. Hazard. Mat.*, **177**, 1-3, 70-80. https://doi.org/10.1016/j.jhazmat.2009.12.047

Saratale RG, Saratale GD, Chang JS, Govindwar SP, (2019a) Bacterial decolorization and degradation of azo dyes: A review. *J. Taiwan Inst. Chem. Engin.* **42**(1), 138-157. https://doi.org/10.1016/j.jtice.2010.06.006

Sirés I, Brillas E, (2012) Remediation of water pollution caused by pharmaceutical residues based on electrochemical separation and degradation technologies: a review. *Environ. Int.*, **40**, 212-229.

Thi TTL, Ta HS, Van KL, (2021) Activated carbons from coffee husk: Preparation, characterization, and reactive red 195 adsorption. *J. Chem. Res.,* **45**(5-6), 380-394. https://doi.org/10.1177/1747519820970469

Verma AK, Dash RR, Bhunia P, (2021) A review on chemical coagulation/flocculation technologies for removal of colour from textile wastewaters. *J. Environ. Manag.*, **93**(1), 154-168. https://doi.org/10.1016/j.jenvman.2011.09.012

Wong S, Ghafar NA, Ngadi N (2020) Effective removal of anionic textile dyes using adsorbent synthesized from coffee waste. *Scientific Reports*, **10**, 2928.

Yan X, Wang J, Li X, (2018) Influence of pH on adsorption behavior in aqueous solutions. *J. Environ. Chem.*, **45**(2), 123-131.

Zahir A, Mahmood U, Aslam Z, Naseem S, Obayomi, KS, Kumar P, Saptoro A, Lau SY, Tiong ANT, Abid S, (2024) Growth of novel cinnamon-bentonite loaded chitosan nanospikes for the confiscation of congo red: adsorption studies and ANN modeling. *J. Poly. & Environ.*, **32**, 1764–1783. https://doi.org/10.1007/s10924-023-03071-x

Zhang EL, Sun XJ, Liu XT, Wang QD, (2015) Morphology controlled synthesis of α-FeOOH crystals and their shape-dependent adsorption for decontamination of congo red dye. *Mat. Res. Innov.*, **19**, 385–391. https://doi.org/10.1179/1433075X15Y.0000000019

Zhu Y, Liu H, Tang J, (2020) The role of pH_{pzc} in adsorption mechanisms for heterogeneous adsorbents. *Chem. Engin. J.*, **375**, 121974.

Zuorro A, Lavecchia R, (2020) Coffee grounds as an alternative biosorbent for the removal of heavy metals from aqueous solutions: A review. *Sustainability,* **12**(6), 2406. https://doi.org/10.3390/su12062406